

Adaptive stimulus selection for multi-alternative psychometric functions with lapses

Ji Hyun Bak^{1,2} and Jonathan W. Pillow³

¹School of Computational Sciences, Korea Institute for Advanced Study, Seoul, Korea; ²Department of Physics, Princeton University, NJ, USA;

³Department of Psychology and Princeton Neuroscience Institute, Princeton University, NJ, USA

(Dated: February 6, 2018)

Psychometric functions (PFs) quantify how external stimuli affect behavior and play an important role in building models of sensory and cognitive processes. Adaptive stimulus selection methods seek to select stimuli that are maximally informative about the PF given data observed so far in an experiment and thereby reduce the number of trials required to estimate the PF. Here we develop new adaptive stimulus selection methods for flexible PF models in tasks with two or more alternatives. We model the PF with a multinomial logistic regression mixture model that incorporates realistic aspects of psychophysical behavior, including lapses (trials where the observer ignores the stimulus) and omissions (trials where the observer “opts out” or fails to provide a valid response). We propose an information-theoretic criterion for stimulus selection and develop computationally efficient methods for inference and stimulus selection based on semi-adaptive Markov Chain Monte Carlo (MCMC) sampling. We apply these methods to data from macaque monkeys performing a multi-alternative motion discrimination task, and show in simulated experiments that our method can achieve a substantial speed-up over random designs. These advances will reduce the data needed to build accurate models of multi-alternative PFs and can be extended to high-dimensional PFs that would be infeasible to characterize with standard methods.

Keywords: adaptive stimulus selection, sequential optimal design, Bayesian adaptive design, psychometric function, closed-loop experiments

1 Introduction

2 Understanding the factors governing psychophysical behavior is
3 a central problem in neuroscience and psychology. Although ac-
4 curate quantification of the behavior is an important goal in it-
5 self, psychophysics provides an important tool for interrogating
6 the mechanisms governing sensory and cognitive processing in the
7 brain. As new technologies allow direct manipulations of neural
8 activity in the brain, there is a growing need for methods that can
9 characterize rapid changes in psychophysical behavior.

10 In a typical psychophysical experiment, an observer is trained to
11 report judgements about a sensory stimulus by selecting a response
12 from among two or more alternatives. The observer is assumed to
13 have an internal probabilistic rule governing these decisions; this

probabilistic map from stimulus to response is called the observer’s
psychometric function. Because the psychometric function is not
directly observable, it must be inferred from multiple observations
of stimulus-response pairs. However, such experiments are costly
due to the large numbers of trials typically required to obtain good
estimates of psychometric functions. Therefore, a problem of ma-
jor practical importance is to develop efficient experimental de-
signs that can minimize the amount of data required to accurately
infer an observer’s psychometric function.

Bayesian adaptive stimulus selection. A powerful ap-
proach for improving the efficiency of psychophysical experiments
is to design the data collection process so that the stimulus is adap-
tively selected on each trial by maximizing a suitably defined ob-
jective function (MacKay, 1992). Such methods are known by a

28 variety of names, including “active learning”, “adaptive or sequen-
29 tial optimal experimental design”, and “closed-loop experiments.”

30 Bayesian approaches to adaptive stimulus selection define op-
31 timality of a stimulus in terms of its expected ability to improve
32 the posterior distribution over the psychometric function, e.g., by
33 reducing its variance or entropy. The three key ingredients of
34 a Bayesian adaptive stimulus selection method are (Chaloner &
35 Verdinelli, 1995; Pillow & Park, 2016):

- 36 • **model** - parametrizes the psychometric function of interest;
- 37 • **prior** - captures initial beliefs about model parameters;
- 38 • **utility function** - quantifies the usefulness of a hypothetical
39 stimulus-response pair for improving the posterior.

40 Sequential algorithms for adaptive Bayesian experiments rely on
41 repeated application of three basic steps: (1) data collection (stim-
42 ulus presentation and response measurement); (2) inference (pos-
43 terior updating using data from the most recent trial); and (3) se-
44 lection of an optimal stimulus for the next trial by maximizing ex-
45 pected utility (see Fig. 1A). The inference step involves updating
46 the posterior distribution over the model parameters according to
47 Bayes rule with data from the most recent trial. Stimulus selection
48 involves calculating the expected utility (i.e., the expected improve-
49 ment in the posterior) for a set of candidate stimuli, averaging over
50 the responses that might be elicited for each stimulus, and select-
51 ing the stimulus for which the expected utility is highest. Example
52 utility functions include the negative trace of the posterior covari-
53 ance (corresponding to the sum of the posterior variances for each
54 parameter) and the mutual information or information gain (which
55 corresponds to minimizing the entropy of the posterior).

56 Methods for Bayesian adaptive stimulus selection have been de-
57 veloped over several decades in a variety of different disciplines.
58 If we focus on the specific application of estimating psychomet-
59 ric functions, the field goes back to the QUEST algorithm (Watson
60 & Pelli, 1983) for estimating discrimination thresholds, and the
61 Ψ method (Kontsevich & Tyler, 1999) for estimating both thresh-
62 old and slope of a psychometric function. These methods have

been extended to models with more parameters (Kujala & Lukka, 63
2006; Lesmes, Lu, Baek, & Albright, 2010; Prins, 2013), in partic- 64
ular models with multi-dimensional stimuli (DiMattina, 2015; Ku- 65
jala & Lukka, 2006; Watson, 2017). In parallel, the development 66
of Bayesian methods for inferring psychometric functions (Kuss, 67
Jäkel, & Wichmann, 2005; Prins, 2012; Wichmann & Hill, 2001) 68
have enlarged the space of statistical models for psychophysical 69
phenomena. 70

A variety of recent advances have arisen in sensory neuroscience 71
or neurophysiology, driven by the development of efficient in- 72
ference techniques for neural encoding models (Lewi, Butera, & 73
Paninski, 2009; Park, Horwitz, & Pillow, 2011) or model compar- 74
ison and discrimination methods (Cavagnaro, Myung, Pitt, & Ku- 75
jala, 2010; DiMattina & Zhang, 2011; Kim, Pitt, Lu, Steyvers, & 76
Myung, 2014). These advances can in many cases be equally well 77
applied to psychophysical experiments. 78

One limitation of previous work is that has often considered only 79
a restricted set of tractable psychometric function models. Stan- 80
dard choices including the logistic regression model (Chaloner & 81
Larntz, 1989; Zocchi & Atkinson, 1999), the Weibull distribution 82
function (Watson & Pelli, 1983), and the cumulative function of 83
Gaussian distribution (Kontsevich & Tyler, 1999). In order for 84
adaptive stimulus selection to be useful in realistic experimental 85
settings, however, it is crucial to incorporate the system-specific 86
features that are not fully captured by the standard models. 87

Our contributions. In this paper, we develop methods for adap- 88
tive stimulus selection in psychophysical experiments that are ap- 89
plicable to realistic models of human and animal psychophysical 90
behavior. Our first contribution is to develop a model of psy- 91
chometric function that incorporates two common “anomalies” of 92
decision-making behavior: omission and lapse. By recognizing 93
omission, we bring to light the well-known (but often ignored) 94
possibility that an observer does not choose any of the provided 95
set of actions, *omitting* the response for the trial. By recognizing 96
lapse, we take into account the possibility that the observer makes 97
occasional errors on easy trials due to momentary lapses in con- 98

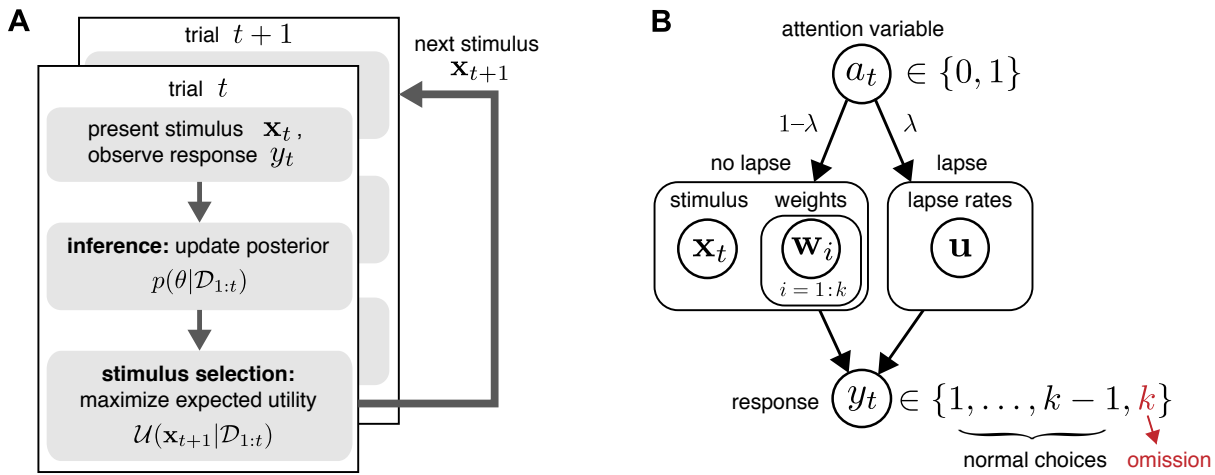


Figure 1: **(A)** Schematic of Bayesian adaptive stimulus selection. On each trial: (1) a stimulus is presented and response is observed; (2) the posterior over the parameters θ is updated using all data collected so far in the experiment \mathcal{D}_t ; and (3) the stimulus that maximizes the expected utility (in our case, information gain) is selected for the next trial. **(B)** A graphical model illustrating a hierarchical psychophysical observer model that incorporates lapses and “omissions”. lapse. On each trial, a latent attention or lapse variable a_t is drawn from a Bernoulli distribution with parameter λ , to determine whether the observer attends to the stimulus \mathbf{x}_t on that trial or lapses. With probability $1 - \lambda$, the observer attends to the stimulus ($a_t = 0$), and the response y_t is drawn from a multinomial logistic regression model, where the probability of choosing option i is proportional to $\exp(\mathbf{w}_i^T \mathbf{x}_t)$. With probability λ , the observer lapses ($a_t = 1$) and selects a choice from a (stimulus-independent) response distribution governed by parameter vector \mathbf{u} . So-called “omission” trials, in which the observer does not select one of the valid response options, are modeled with an additional response category $y_t = k$.

99 centration or memory (Kuss et al., 2005; Wichmann & Hill, 2001).
 100 Although it is widely understood among experimental researchers
 101 that both effects can be significant in real animal behavior, these
 102 are often ignored in analysis, and in particular, are not considered
 103 by previous methods for adaptive stimulus selection. Here we in-
 104 corporate these two phenomena explicitly, as explained in more
 105 details in Section Psychometric Function Model.

106 As the model complexity grows by adding extra features, on the
 107 other hand, the increasing challenge is to infer the model param-
 108 eters efficiently (in finite computation time), flexibly (under small-
 109 data situations, and/or with non-concave models), and accurately.
 110 Our second contribution is to develop efficient inference methods
 111 that are fast enough for real-time closed-loop experiments. We dis-
 112 cuss two methods for posterior inference, one based on a Gaussian
 113 approximation of the posterior and another based on MCMC sam-
 114 pling, in Section Posterior inference.

115 Our work therefore combines a more realistic model of the psy-

116 chometric function and efficient methods for posterior inference
 117 and evaluation of an information-theoretic utility function. We de-
 118 scribe two different algorithms for adaptive stimulus selection Sec-
 119 tion Adaptive Stimulus Selection Methods, one based on a Gaus-
 120 sian approximation to the posterior and a second based on MCMC
 121 sampling. Finally, in Results, we apply our algorithms to real data
 122 in simulated closed-loop experiments. We show that our methods
 123 confer a substantial reduction in the number of trials required to es-
 124 timate multi-alternative psychophysical functions, and discuss ex-
 125 tensions applicable to experiments with multi-dimensional stimuli.

Psychometric Function Model

126 Here we develop a flexible model of psychometric function (PF)
 127 for describing realistic decision-making behavior, starting with a
 128 classical multinomial logistic (MNL) model (Glonek & McCul-
 129 lagh, 1995). We show how omission can be naturally incorporated
 130

131 into the framework with multiple alternatives. We then develop a
132 hierarchical extension of the model that incorporates lapses (see
133 Fig. 1B).

134 **Multinomial logistic model.** We consider the setting where the
135 observer is presented with a stimulus $\mathbf{x} \in \mathbb{R}^d$ and selects a response
136 $y \in \{1, \dots, k\}$ from one of k discrete choices on each trial. We will
137 assume the stimulus is represented internally by some (possibly
138 non-linear) feature vector $\phi(\mathbf{x})$, which we will write simply as ϕ
139 for notational simplicity.

140 In the multinomial logistic model, the probability p_i of each pos-
141 sible outcome $i \in \{1, \dots, k\}$ is determined by the dot product
142 between the feature ϕ and a vector of weights \mathbf{w}_i according to:

$$143 \quad p_i = \frac{\exp(\mathbf{w}_i^\top \phi)}{\sum_{j=1}^k \exp(\mathbf{w}_j^\top \phi)}, \quad (1)$$

144 where the denominator ensures that these probabilities sum to 1,
145 $\sum_{i=1}^k p_i = 1$. The function from stimulus to a probability vector
146 over choices, $\mathbf{x} \mapsto (p_1, \dots, p_k)$, is the psychometric function, and
147 the set of weights $\{\mathbf{w}_i\}_{i=1}^k$ are its parameters. Note that the model
148 is over-parameterized when written this way, since the requirement
149 that probabilities sum to 1 removes one degree of freedom from
150 the probability vector. Thus, we can without loss of generality fix
151 one of the weight vectors to zero, for example $\mathbf{w}_k = \mathbf{0}$, so that
152 the denominator in (eq. 1) becomes $z = 1 + \sum_{j=1}^k \exp(\mathbf{w}_j^\top \phi)$ and
153 $p_k = 1/z$.

154 We consider the feature vector ϕ to be a known function of the
155 stimulus \mathbf{x} , even when the dependence is not written explicitly.
156 For example, we can consider a simple form of feature embedding,
157 $\phi(\mathbf{x}) = [1, \mathbf{x}^\top]^\top$, corresponding to a linear function of the stim-
158 ulus plus an offset. In this case, the weights for the i 'th choice
159 would correspond to $\mathbf{w}_i = [b_i, \mathbf{a}_i^\top]^\top$, where b_i is the offset or bias
160 for the i 'th choice, and \mathbf{a}_i are the linear weights governing sensi-
161 tivity to \mathbf{x} . The resulting choice probability has the familiar form,
162 $p_i \propto \exp(b_i + \mathbf{a}_i^\top \mathbf{x})$. Nonlinear stimulus dependencies can be
163 incorporated by including nonlinear functions of \mathbf{x} in the feature
164 vector $\phi(\mathbf{x})$ (Knoblauch & Maloney, 2008; Murray, 2011; Neri &
165 Heeger, 2002).

It is useful to always work with a normalized stimulus space,
in which the mean of each stimulus component x_α over the stim-
ulus space is $\langle x_\alpha \rangle = 0$, and the standard deviation $\text{std}(x_\alpha) = 1$.
This normalization ensures that the values of the weight parameters
are defined in more interpretable ways. The zero-mean condition
ensures that the bias b is the expectation value of log probability
over all possible stimuli. The unit-variance condition means that
the effect of moving a certain distance along one dimension of the
weight space is comparable to the moving the same distance in an-
other dimension, again averaged over all possible stimuli. In other
words, we are justified to use the same unit along all dimensions of
the weight space.

178 **Modeling omission as an additional category.** Even in
179 “binary” tasks with only two possible choices per trial, there is of-
180 ten an implicit third choice, which is to make no response, make
181 an illegal response, or interrupt the trial at some point before the
182 response period. For example, animals are often required to main-
183 tain an eye position or a nose poke, or wait for a “go” cue be-
184 fore reporting a choice. Trials on which the animal fails to obey
185 these instructions, referred to as “violations” or “omissions”, and
186 are typically discarded from analysis. However, such trials have
187 clear relevance to the quantitative study of psychophysical behav-
188 ior, and may reflect aspects of motivation or attentional state that
189 are worth studying in their own right. Luckily, the multinomial log-
190 istic model provides a natural framework for incorporating omis-
191 sion or no-response trials.

Here we model omissions explicitly as one of the possible
choices the observer can choose. Because the multinomial logis-
tic model has a flexible number of choices, this is as simple as
adding an extra or $(k + 1)$ 'st choice to the model. One can even
extend the model to consider different kinds of omissions, e.g., al-
lowing choice $k + 1$ to reflect fixation period violations and choice
 $k + 2$ to reflect failure to report a choice during the response win-
dow. Henceforth, we will simply let k reflect the total number of
choices, including omission, as illustrated in Fig. 1B.

201 **Modeling lapse with a mixture model.** Another important
202 feature of real psychophysical observers is the tendency to occa-
203 sionally make errors that are independent of the stimulus. Such
204 errors, commonly known as “lapses” in the psychophysical liter-
205 ature, may reflect lapses in attention or memory of the response
206 categories, or “button-press errors” in executing an intended motor
207 response. Lapses are most easily identified by errors on “easy” tri-
208 als, that is, trials that should be performed perfectly if the observer
209 were paying attention.

210 Although lapse rates are supposed to be small enough in a
211 well-performed psychometric experiment (Carandini & Church-
212 land, 2013), in reality they may be substantial depending on the
213 type of experiment being performed, especially in non-primates or
214 in more complicated tasks. Lapses affect the psychometric func-
215 tion by causing it to saturate above 0 and below 1, so that “perfect”
216 performance is never achieved even for the easiest trials. Failure to
217 incorporate lapses into the PF model may therefore bias estimates
218 of sensitivity, as quantified by PF slope or threshold (Prins, 2012;
219 Wichmann & Hill, 2001).

220 To model lapses, we use a mixture model that treats the ob-
221 server’s choice on each trial as coming from one of two probability
222 distributions: a stimulus-dependent distribution (governed by the
223 multinomial logistic model) and stimulus-independent distribution
224 (reflecting a fixed probability of choosing any option when “laps-
225 ing”, or ignoring the stimulus). Simpler versions of such mixture
226 model have been proposed previously (Kuss et al., 2005).

227 Fig. 1B shows a schematic of the resulting model. On each trial,
228 a Bernoulli random variable $a \sim \text{Ber}(\lambda)$ governs whether the ob-
229 server lapses: with probability λ and the observer lapses (i.e., ig-
230 nores the stimulus), and with probability $1 - \lambda$, and the observer at-
231 tends to the stimulus. If the observer lapses ($a = 1$), the response is
232 drawn according to fixed probability distribution (c_1, \dots, c_k) gov-
233 erning the probability of selecting options 1 to k , where $\sum c_i = 1$.
234 If the observer does not lapse ($a = 0$), the observer selects a re-
235 sponse according to the multinomial logistic model. Under this
236 model, the conditional probability of choosing option i given the

stimulus can be written:

$$p_i = (1 - \lambda)q_i + \lambda c_i, \quad q_i = \frac{\exp(\mathbf{w}_i^\top \phi)}{\sum_j \exp(\mathbf{w}_j^\top \phi)} \quad (2)$$

239 where q_i is the lapse-free probability probability under the classical
240 MNL model (eq. 1).

241 It is convenient to re-parameterize this model so that λc_i , the
242 conditional probability of choosing the i ’th option due to a lapse,
243 is written

$$\lambda c_i = \frac{\exp(u_i)}{1 + \sum_j \exp(u_j)}, \quad (3)$$

245 where each auxiliary lapse parameter u_i is proportional to the log
246 probability of choosing option i due to lapse. The lapse-conditional
247 probabilities of each choice, c_i , and the total lapse probability, λ ,
248 are respectively

$$c_i = \frac{\exp(u_i)}{\sum_j \exp(u_j)}, \quad \lambda = \sum_i \frac{\exp(u_i)}{1 + \sum_j \exp(u_j)}. \quad (4)$$

250 Because each u_i lives on the entire real line, fitting can be carried
251 out with unconstrained optimization methods, although adding rea-
252 sonable constraints may improve performance in some cases. The
253 full parameter vector of the resulting model is $\theta = [\mathbf{w}^\top, \mathbf{u}^\top]^\top$,
254 which includes k additional lapse parameters $\mathbf{u} = \{u_1, \dots, u_k\}$.
255 Note that in some cases it might be desirable to assume lapse
256 choices obey a uniform distribution, where the probability of each
257 option is $c_i = 1/k$. For this simplified “uniform-lapse” model we
258 need only a single lapse parameter u .

259 Our model provides a general and practical parametrization of
260 tuning curves with lapses. Although previous work has considered
261 the problem of modeling lapses in psychophysical experiments,
262 most assumed the the simplified uniform-lapse model where all
263 options are equally likely during lapses. Earlier approaches have
264 often assumed either that the lapse probability was known a priori
265 (Kontsevich & Tyler, 1999), or was fit by a grid search over a small
266 set of candidate values (Wichmann & Hill, 2001). We instead take
267 a Bayesian approach to inferring lapse parameters, following previ-
268 ous work from (Kuss et al., 2005; Prins, 2012). Our parameteriza-
269 tion (eq. 3) has the advantage that the there is no need to constrain

270 the support of the lapse parameters u_i . These parameters' relation-
271 ship to lapse probabilities c_i takes the same ("softmax") functional
272 form as the multinomial logistic model, placing both sets of param-
273 eters on an equal footing.

274 Posterior inference

275 Bayesian methods for adaptive stimulus selection require the pos-
276 terior distribution over model parameters given the data observed
277 so far in an experiment. The posterior distribution results from the
278 combination of two ingredients: a prior distribution $p(\boldsymbol{\theta})$, which
279 captures prior uncertainty about the model parameters $\boldsymbol{\theta}$, and a
280 likelihood function $p(\{y_s\}|\{\mathbf{x}_s\}, \boldsymbol{\theta})$, which captures information
281 about the parameters from the data $\{(\mathbf{x}_s, y_s)\}$, $s = 1, \dots, t$, con-
282 sisting of stimulus-response pairs observed up to the current time
283 bin t .

284 Unfortunately, the posterior distribution for our model has no
285 analytic form. We therefore describe two methods for approximate
286 posterior inference: one relying on a Gaussian approximation to
287 the posterior, known as the Laplace approximation, and a second
288 one based on MCMC sampling.

289 **Prior.** The prior distribution specifies our beliefs about model
290 parameters before we have collected any data, and serves to reg-
291 ularize estimates obtained from small amounts of data, e.g., by
292 shrinking estimated weights toward zero. Typically we want the
293 prior to be weak enough that the likelihood dominates the poste-
294 rior for reasonable-sized datasets. However, the choice of prior is
295 especially important in adaptive stimulus selection settings because
296 it determines the effective volume of the search space (Park & Pil-
297 low, 2012; Park, Weller, Horwitz, & Pillow, 2014). For example, if
298 the weights are known to exhibit smoothness, then a correlated or
299 smoothness-inducing prior can improve the performance of adap-
300 tive stimulus selection because the effective size (or entropy) of the
301 parameter space is much smaller than under an independent prior
302 (Park & Pillow, 2012).

303 In this study, we use a generic independent, zero-mean Gaussian

prior over the weight vectors

$$p(\mathbf{w}_i) = \mathcal{N}(\mathbf{0}, \sigma^2 I), \quad (5)$$

306 for all $i \in (1, \dots, k)$, with a fixed standard deviation σ . This choice
307 of prior is appropriate when the regressors $\{\mathbf{x}\}$ are standardized,
308 since any single weight can take values that allow for a range of
309 psychometric function shapes along that axis, from flat ($w = 0$) to
310 steeply decreasing ($w = -2\sigma$) or increasing ($w = +2\sigma$). We
311 used $\sigma = 3$ in the simulated experiments in Results. For the
312 lapse parameters $\{u_i\}$, we used a uniform prior over the range
313 $[\log(0.001), 0]$, so that each lapse probability λc_i is bounded be-
314 tween 0.001 and 1/2. We set the lower range constraint below
315 $1/N$, where $N = 100$ is the number of observed trials in our sim-
316 ulations, since we cannot reasonably infer lapse probabilities with
317 precision finer than $1/N$. The upper range constraint gives maxi-
318 mal lapse probabilities of $1/(k + 1)$ if all u_i take on the maximal
319 value of 0.

320 **Psychometric function likelihood.** The likelihood is the con-
321 ditional probability of the data as a function of the model param-
322 eters. Although we have thus far considered the response variable
323 y to be a scalar taking values in the set $\{1, \dots, k\}$, it is more con-
324 venient to use a so-called "one-hot" representation, in which the
325 response variable \mathbf{y} for each trial is a length- k vector with one 1
326 and k zeros, where the position of the 1 in this vector indicates the
327 category chosen. For example, in a task with four possible options
328 per trial, a response vector $\mathbf{y} = [0 \ 0 \ 1 \ 0]$ indicates a trial on which
329 the observer selected the third option.

330 With this parametrization, the log-likelihood function for a sin-
331 gle trial can be written

$$\log p(\mathbf{y}|\mathbf{x}, \boldsymbol{\theta}) = \sum_i y_i \log p_i(\mathbf{x}, \boldsymbol{\theta}) = \mathbf{y}^\top \log \mathbf{p}(\mathbf{x}, \boldsymbol{\theta}), \quad (6)$$

333 where $p_i(\mathbf{x}, \boldsymbol{\theta})$ denotes the probability $p(y_i = 1|\mathbf{x}, \boldsymbol{\theta})$ under the
334 model (eq. 1), and $\mathbf{p}(\mathbf{x}, \boldsymbol{\theta}) \equiv [p_1(\mathbf{x}, \boldsymbol{\theta}), \dots, p_k(\mathbf{x}, \boldsymbol{\theta})]^\top$ denotes
335 the vector of probabilities for a single trial.

336 In the classical (lapse-free) multinomial logistic model, where
337 $\boldsymbol{\theta} = \{\mathbf{w}_i\}$, the log likelihood is a concave function of $\boldsymbol{\theta}$, which

338 guarantees that numerical optimization of the log-likelihood will
339 find a global optimum. With a finite lapse rate, however, the log
340 likelihood is no longer provably concave. (See [Appendix A](#)).

341 **Posterior distribution.** The log-posterior can be written as the
342 sum of log-prior and log-likelihood summed over trials, plus a con-
343 stant:

$$344 \log p(\boldsymbol{\theta}|\mathcal{D}_t) = \log p(\boldsymbol{\theta}) + \sum_{s=1}^t \log p(\mathbf{y}_s|\mathbf{x}_s, \boldsymbol{\theta}) + c, \quad (7)$$

345 where $\mathcal{D}_t \equiv \{\mathbf{x}_s, \mathbf{y}_s\}_{s=1}^t$ denotes the accumulated data up to trial
346 t and $c = -\log(\int p(\boldsymbol{\theta}) \prod_s p(\mathbf{y}_s|\mathbf{x}_s) d\boldsymbol{\theta})$ is a normalization con-
347 stant that does not depend on the parameters $\boldsymbol{\theta}$. Because this con-
348 stant has no tractable analytic form, we rely on two alternate meth-
349 ods for obtaining a normalized posterior distribution.

350 **Inference via Laplace approximation.** The Laplace approx-
351 imation is a well-known Gaussian approximation to the posterior
352 distribution, which can be derived from a second-order Taylor se-
353 ries approximation to the log-posterior around its mode ([Bishop,](#)
354 [2006](#)).

355 Computing the Laplace approximation involves a two-step pro-
356 cedure. The first step is to perform a numerical optimization of
357 $\log p(\boldsymbol{\theta}|\mathcal{D}_t)$ to find the posterior mode, or maximum a posteriori
358 (MAP) estimate of $\boldsymbol{\theta}$. This vector, given by

$$359 \hat{\boldsymbol{\theta}}_t = \underset{\boldsymbol{\theta}}{\operatorname{argmax}} \log p(\boldsymbol{\theta}) + \sum_{s=1}^t \log p(\mathbf{y}_s|\mathbf{x}_s, \boldsymbol{\theta}), \quad (8)$$

360 provides the mean of the Laplace approximation. Because we can
361 explicitly provide the gradient and Hessian of the log likelihood
362 (see [Appendix A](#)) and log-prior, this optimization can be carried
363 efficiently via Newton-Raphson or trust region methods.

364 The second step is to compute the second derivative (the Hes-
365 sian matrix) of the log-posterior at the mode, which provides the
366 inverse covariance of the Gaussian. This gives us a local Gaussian
367 approximation of the posterior, centered at the posterior mode:

$$368 p(\boldsymbol{\theta}|\mathcal{D}_t) \approx \mathcal{N}(\hat{\boldsymbol{\theta}}_t, C_t), \quad (9)$$

369 where covariance $C_t = -H_t^{-1}$ is the inverse Hessian of the log
370 posterior, $H_t(i, j) = \partial^2(\log p(\boldsymbol{\theta}|\mathcal{D}_t))/(\partial\theta_i\partial\theta_j)$, evaluated at $\hat{\boldsymbol{\theta}}_t$.

Note that when the log-posterior is concave (i.e., when the
371 model does *not* contain lapse), numerical optimization is guaran-
372 teed to find a global maximum of the posterior. Log-concavity
373 also strengthens the rationale for using the Laplace approximation,
374 since the true and approximate posterior are both log-concave den-
375 sities centered on the true mode ([Paninski et al., 2010](#); [Pillow, Ah-](#)
376 [madian, & Paninski, 2011](#)). However, when the model incorporates
377 lapses, these guarantees no longer apply, motivating the use of al-
378 ternate methods for approximating the posterior. 379

Inference via MCMC sampling. A second approach to infer-
380 ence is to generate samples from the posterior distribution over
381 the parameters via Markov Chain Monte Carlo (MCMC) sampling.
382 Sampling-based methods are typically more computationally in-
383 tensive than the Laplace approximation, but may be warranted
384 when the posterior is not provably log-concave (as is the case when
385 lapse rates are non-zero) and therefore not well approximated by a
386 single Gaussian. 387

The basic idea in MCMC sampling is to set up an easy-to-sample
388 Markov Chain that has the posterior as its stationary distribution.
389 Sampling from this chain produces a dependent sequence of pos-
390 terior samples: $\{\boldsymbol{\theta}_m\} \sim p(\boldsymbol{\theta}|\mathcal{D}_t)$, which can be used to evaluate
391 posterior expectations via Monte Carlo integrals: 392

$$393 \mathbb{E}[f(\boldsymbol{\theta})] \approx \frac{1}{M} \sum_{m=1}^M f(\boldsymbol{\theta}_m), \quad (10)$$

394 for any function $f(\boldsymbol{\theta})$. The mean of the posterior is obtained from
395 setting $f(\boldsymbol{\theta}) = \boldsymbol{\theta}$, although for adaptive stimulus selection we will
396 be interested in the full shape of the posterior. 396

The Metropolis-Hastings (MH) algorithm is perhaps the sim-
397 plest and most widely-used MCMC sampling method ([Metropo-](#)
398 [lis, Rosenbluth, Rosenbluth, Teller, & Teller, 1953](#)). It generates
399 samples via a proposal distribution centered on the current sample
400 (see [Appendix B](#)). The choice of proposal distribution is critical to
401 the efficiency of the MH algorithm, since this governs the rate of
402 “mixing”, or the the number of Markov Chain samples required to
403 obtain independent samples from the posterior distribution ([Rosen-](#)
404 [thal, 2011](#)). Faster mixing implies that fewer samples M are re-
405

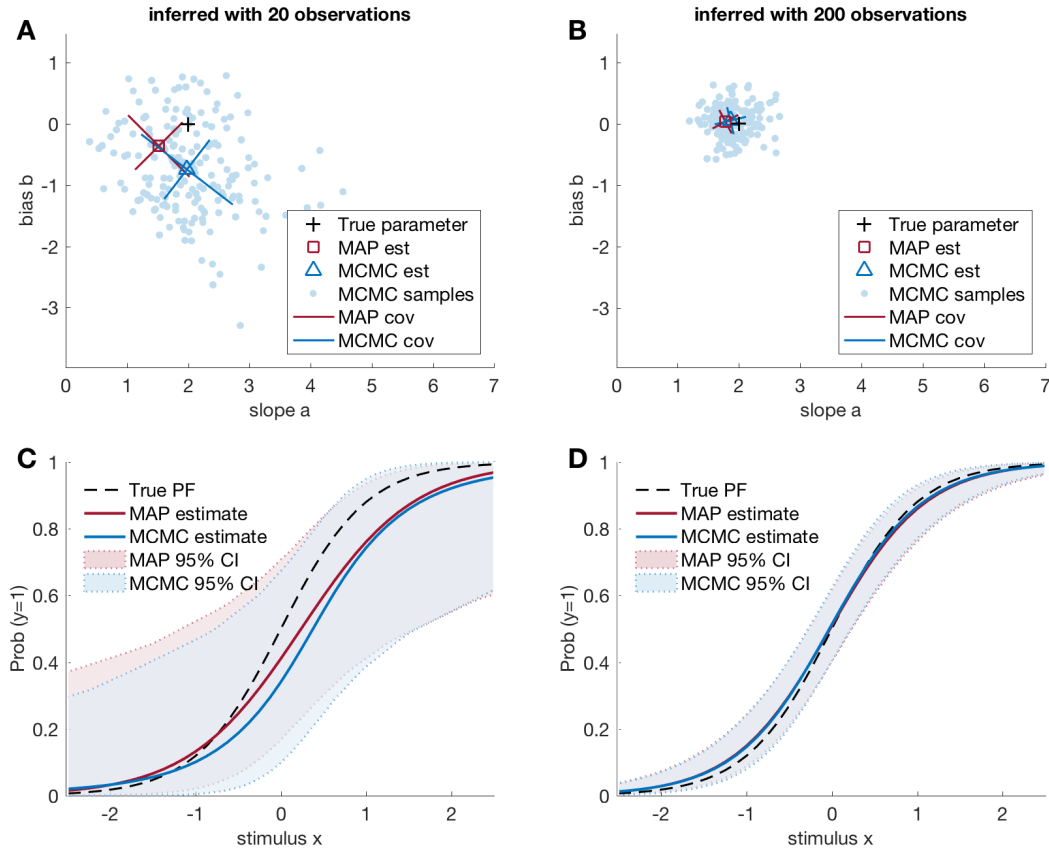


Figure 2: Inferring the psychometric function. Example of a psychometric problem, with a lapse-free binomial logistic model $f(v) = e^v / (1 + e^v)$. Given a 1D stimulus, a response were drawn from a “true” model $P(y = 1) = f(b + ax)$ with two parameters, slope $a = 2$ and bias $b = 0$. **(A-B)** Viewing on the parameter space, the posterior distributions become sharper (and closer to the true parameter values) as the dataset size N increases. Shown at a small **(A)** $N = 20$ and a large **(B)** $N = 200$. For the MAP estimate, the mode of the distribution is marked with a square, and the two standard deviations (“widths”) of its Gaussian approximation are shown with bars. For the MCMC sampling method, all $M = 500$ samples of the chain are shown in dots, the sample mean with a triangle, and the widths with the bars. The widths are the standard deviations along the principal directions of the sampled posterior (eigenvectors of the covariance matrix; not necessary aligned with the $a - b$ axes). **(C-D)** The accuracy of the estimated PF improves with the number of observations N , using either of the two posterior inference methods (MAP-based and sampling-based). Shown at a small **(C)** $N = 20$ and a large **(D)** $N = 200$. The two methods are highly consistent in this simple case, especially when N is large enough.

quired to obtain an accurate approximation to the posterior.

Here we propose a semi-adaptive Metropolis-Hastings algorithm, developed specifically for the current context of sequential learning. Our approach is based on an established observation that the optimal width of the proposal distribution should be proportional to the typical length scale of the distribution being sampled (Gelman, Roberts, & Gilks, 1996; Roberts, Gelman, & Gilks, 1997). Our algorithm is motivated by the adaptive Metropolis algorithm (Haario, Saksman, & Tamminen, 2001), where the proposal distribution is updated at each proposal within a single chain; here we do not adapt the proposal within chains, but rather after each trial. Specifically, we set the covariance of a Gaussian proposal distribution to be proportional to the covariance of the samples from the previous trial, using the scaling factor of Haario et al. (2001). See Appendix B for details. The adaptive algorithm takes advantage of the fact that the posterior cannot change too much between trials, since it changes only by a single-trial likelihood term on each trial.

Adaptive Stimulus Selection Methods

As data are collected during the experiment, the posterior distribution becomes narrower due to the fact that each trial carries some additional information about the model parameters. (See Fig. 2.) This narrowing of the posterior is directly related to information gain. A stimulus that produces no expected narrowing of the posterior is, by definition, uninformative about the parameters. On the other hand, a stimulus that (on average) produces a large change in the current posterior is an informative stimulus. Selecting informative stimuli will reduce the number of stimuli required to obtain a narrow posterior, which is the essence of adaptive stimulus selection methods. In this section, we introduce a precise measure of information gain between a stimulus and the model parameters, and propose an algorithm for selecting stimuli to maximize it.

Infomax criterion for stimulus selection. At each trial, we present a stimulus \mathbf{x} and observe the outcome \mathbf{y} . After t trials, the

expected gain in information from a stimulus \mathbf{x} is equal to the mutual information between \mathbf{y} and the model parameters $\boldsymbol{\theta}$, given the data \mathcal{D}_t observed so far in the experiment. We denote this conditional mutual information:

$$I_t(\boldsymbol{\theta}; \mathbf{y}|\mathbf{x}) = \iint d\boldsymbol{\theta} d\mathbf{y} p(\boldsymbol{\theta}, \mathbf{y}|\mathbf{x}, \mathcal{D}_t) \log \frac{p(\boldsymbol{\theta}, \mathbf{y}|\mathbf{x}, \mathcal{D}_t)}{p(\boldsymbol{\theta}|\mathcal{D}_t)p(\mathbf{y}|\mathbf{x}, \mathcal{D}_t)}, \quad (11)$$

where $p(\boldsymbol{\theta}, \mathbf{y}|\mathbf{x}, \mathcal{D}_t)$ is the joint distribution of $\boldsymbol{\theta}$ and \mathbf{y} given a stimulus \mathbf{x} and dataset \mathcal{D}_t , the term $p(\boldsymbol{\theta}|\mathcal{D}_t)$ is the current posterior distribution over the parameters from previous trials, and $p(\mathbf{y}|\mathbf{x}, \mathcal{D}_t) = \int d\boldsymbol{\theta} p(\mathbf{y}|\mathbf{x}, \boldsymbol{\theta})p(\boldsymbol{\theta}|\mathcal{D}_t)$ is known as the posterior-predictive distribution of \mathbf{y} given \mathbf{x} .

It is useful to note that the mutual information can equivalently be written in two other ways involving Shannon entropy. The first is given by:

$$I_t(\boldsymbol{\theta}; \mathbf{y}|\mathbf{x}) = H_t(\boldsymbol{\theta}) - H_t(\boldsymbol{\theta}|\mathbf{y}; \mathbf{x}) \quad (12)$$

where the first term is the entropy of the posterior at time t ,

$$H_t(\boldsymbol{\theta}) = - \int d\boldsymbol{\theta} p(\boldsymbol{\theta}|\mathcal{D}_t) \log p(\boldsymbol{\theta}|\mathcal{D}_t), \quad (13)$$

and the second is the conditional entropy of $\boldsymbol{\theta}$ given \mathbf{y} ,

$$\begin{aligned} H_t(\boldsymbol{\theta}|\mathbf{y}; \mathbf{x}) &= -\mathbb{E}_{\boldsymbol{\theta}, \mathbf{y}} \left[\log p(\boldsymbol{\theta}|\mathbf{y}, \mathbf{x}, \mathcal{D}_t) \right] \\ &= - \iint d\boldsymbol{\theta} d\mathbf{y} p(\boldsymbol{\theta}, \mathbf{y}|\mathbf{x}, \mathcal{D}_t) \log p(\boldsymbol{\theta}|\mathbf{y}, \mathbf{x}, \mathcal{D}_t), \end{aligned} \quad (14)$$

which is the entropy of the updated posterior *after* having observed \mathbf{x} and \mathbf{y} , averaged over draws of \mathbf{y} from the posterior predictive distribution. Written this way, the mutual information can be seen as the expected reduction in posterior entropy from a new stimulus-response pair. Moreover, the first term, $H_t(\boldsymbol{\theta})$, is independent of the stimulus and response on the current trial, so infomax stimulus selection is equivalent to picking the stimulus that minimizes the expected posterior entropy $H_t(\boldsymbol{\theta}|\mathbf{y}; \mathbf{x})$.

A second equivalent expression for the mutual information, which will prove useful for our sampling-based method, is:

$$I_t(\boldsymbol{\theta}; \mathbf{y}|\mathbf{x}) = H_t(\mathbf{y}; \mathbf{x}) - H_t(\mathbf{y}|\boldsymbol{\theta}; \mathbf{x}), \quad (15)$$

475 which is the difference between the marginal entropy of the re-
476 sponse distribution conditioned on \mathbf{x} ,

$$477 \quad H_t(\mathbf{y}; \mathbf{x}) = - \int d\mathbf{y} p(\mathbf{y}|\mathbf{x}, \mathcal{D}_t) \log p(\mathbf{y}|\mathbf{x}, \mathcal{D}_t) \quad (16)$$

478 and the conditional entropy of the response \mathbf{y} given $\boldsymbol{\theta}$, conditioned
479 on the stimulus:

$$480 \quad H_t(\mathbf{y}|\boldsymbol{\theta}; \mathbf{x}) = - \iint d\mathbf{y} d\boldsymbol{\theta} p(\boldsymbol{\theta}, \mathbf{y}|\mathbf{x}, \mathcal{D}_t) \log p(\mathbf{y}|\mathbf{x}, \boldsymbol{\theta}). \quad (17)$$

481 This formulation shows the mutual information to be equal to the
482 difference between the entropy of the marginal distribution of \mathbf{y}
483 conditioned on \mathbf{x} (with $\boldsymbol{\theta}$ integrated out) and the average entropy
484 of \mathbf{y} given \mathbf{x} and $\boldsymbol{\theta}$, averaged over the posterior distribution of $\boldsymbol{\theta}$.

485 In a sequential setting where t is the latest trial and $t + 1$ is the
486 upcoming one, the optimal stimulus is the information-maximizing
487 (“infomax”) solution:

$$488 \quad \mathbf{x}_{t+1} = \arg \max_{\mathbf{x}} I_t(\boldsymbol{\theta}; \mathbf{y}|\mathbf{x}). \quad (18)$$

489 Fig. 3 shows an example of a simulated experiment where the stim-
490 ulus was selected adaptively following the infomax criterion.

491 Selecting the optimal stimulus thus requires maximizing the mu-
492 tual information over the set of all possible stimuli $\{\mathbf{x}\}$. Since each
493 evaluation of the mutual information involves a high-dimensional
494 integral over parameter space and response space, this is a highly
495 computationally demanding task. In the next sections, we present
496 two algorithms for efficient infomax stimulus selection based on
497 each of the two approximate inference methods described previ-
498 ously.

499 **Infomax with Laplace approximation.** Calculation of the
500 mutual information is greatly simplified by a Gaussian approxima-
501 tion of the posterior. The entropy of a Gaussian distribution with
502 covariance C is equal to $\frac{1}{2} \log |C|$ up to a constant factor. If we ex-
503 pand the mutual information as in (eq. 12), and recall that we need
504 only minimize the expected posterior entropy after observing the
505 response, the optimal stimulus for time-step $t + 1$ is given by:

$$506 \quad \mathbf{x}_{t+1}^* = \arg \min_{\mathbf{x}} \int d\mathbf{y} p(\mathbf{y}|\mathbf{x}, \mathcal{D}_t) \log |\tilde{C}(\mathbf{x}, \mathbf{y})|, \quad (19)$$

where $\tilde{C}(\mathbf{x}, \mathbf{y})$ is the covariance of the updated (Gaussian) poste-
rior after observing stimulus-response pair (\mathbf{x}, \mathbf{y}) . To evaluate the
updated covariance $\tilde{C}(\mathbf{x}, \mathbf{y})$ under the Laplace approximation, we
would need to numerically optimize the posterior for $\boldsymbol{\theta}$ for each
possible response \mathbf{y} , for any candidate stimulus \mathbf{x} , which would be
computationally infeasible. We therefore use a fast approximate
method for obtaining a closed-form update for $\tilde{C}(\mathbf{x}, \mathbf{y})$ from the
current posterior covariance C_t , following an approach developed
in Lewi et al. (2009). (See Appendix C for details.)

Once we have $\log |\tilde{C}(\mathbf{x}, \mathbf{y})|$ for each given stimulus-observation
pair, we numerically sum this over a set of discrete counts \mathbf{y} that
are likely under the posterior-predictive distribution. This is done
in two steps, by separating the integral in (eq. 19) as:

$$\begin{aligned} & \int d\mathbf{y} p(\mathbf{y}|\mathbf{x}, \mathcal{D}_t) \log |\tilde{C}(\mathbf{x}, \mathbf{y})| \\ &= \int d\boldsymbol{\theta}_t p(\boldsymbol{\theta}_t|\mathcal{D}_t) \int d\mathbf{y} p(\mathbf{y}|\mathbf{x}, \boldsymbol{\theta}_t) \log |\tilde{C}(\mathbf{x}, \mathbf{y})|. \end{aligned} \quad (20)$$

Note that the outer integral is over the current posterior $p(\boldsymbol{\theta}_t|\mathcal{D}_t) \approx$
 $\mathcal{N}(\hat{\boldsymbol{\theta}}_t, C_t)$, which is to be distinguished from the future posterior
 $p(\boldsymbol{\theta}|\mathbf{y}, \mathbf{x}, \mathcal{D}_t) \approx \mathcal{N}(\tilde{\boldsymbol{\theta}}(\mathbf{x}, \mathbf{y}), \tilde{C}(\mathbf{x}, \mathbf{y}))$ whose entropy we are trying
to minimize. Whereas the inner integral is simply a weighted sum
over the set of outcomes \mathbf{y} , the outer integral over the parameter $\boldsymbol{\theta}$
is in general challenging, especially when the parameter space is
high-dimensional. In the case of the standard multinomial logistic
model that does not include lapses, we can exploit the linear struc-
ture of model to reduce this to a lower-dimensional integral over
the space of the linear predictor, which we evaluate numerically
using Gauss-Hermite quadrature (Heiss & Winschel, 2008). (This
integral is 1D for classic logistic regression, and $(k-1)$ -dimensional
for multinomial logistic regression with k classes; see Appendix C
for details.)

When the model incorporates lapses, the full parameter vector
 $\boldsymbol{\theta} = [\mathbf{w}^\top, \mathbf{u}^\top]$ includes the lapse parameters in addition to the
weights \mathbf{w} . In this case, our method with Laplace approximation
may suffer from reduced accuracy due to the fact that the poste-
rior (which is not provably log-concave in this setting) may be less
closely approximated by a Gaussian. For tractability, we choose to

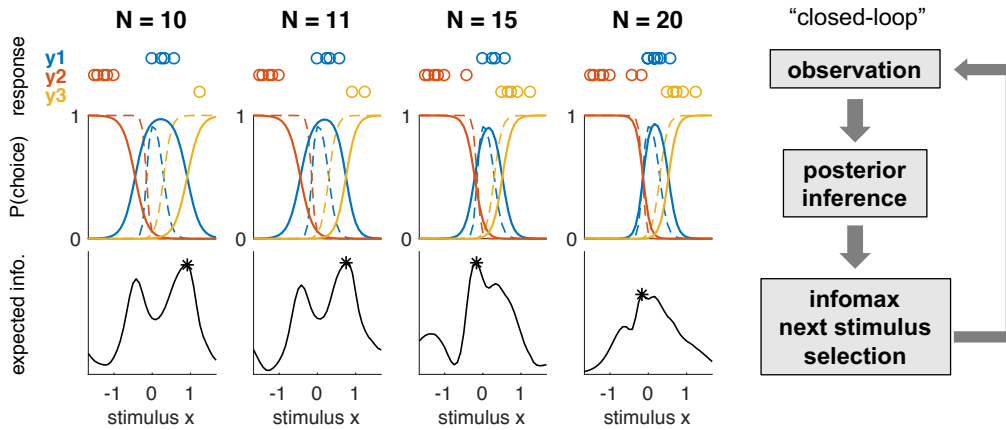


Figure 3: Example of infomax adaptive stimulus selection, simulated with a three-alternatives lapse-free model on 1D stimulus. The figure shows how given a small set of data (the stimulus-response pairs shown in top row), the PFs are estimated based on the accumulated data (middle row), and the next stimulus is chosen to maximize the expected information gain (bottom row). Each column shows the instance after the N observations in a single adaptive stimulus selection sequence, for $N = 10, 11, 15$ and 20 respectively. In the middle row, the estimated PFs (solid lines) quickly approach the true PFs (dashed lines) through the adaptive and optimal selection of stimuli. This example was generated using the Laplace approximation based algorithm, with an independent Gaussian prior over the weights with mean zero and standard deviation $\sigma = 10$.

543 maximize the *partial* information between the observation and the
 544 psychophysical weights, $I(\mathbf{w}; \mathbf{y}|\mathbf{x})$, instead of the full information
 545 $I(\boldsymbol{\theta}; \mathbf{y}|\mathbf{x})$. This is also a reasonable approximation in many cases
 546 where the stimulus-dependent behavior is the primary focus of the
 547 psychometric experiment; the weights \mathbf{w} are of primary interest,
 548 while the lapse \mathbf{u} are usually nuisance parameters. The partial co-
 549 variance $C_{\mathbf{w}\mathbf{w}} = -(\partial^2(\log \mathcal{P})/\partial \mathbf{w}^2)^{-1}$ can be used in place of
 550 the full covariance $C = -(\partial^2(\log \mathcal{P})/\partial \boldsymbol{\theta}^2)^{-1}$. Because the posi-
 551 tive semi-definiteness of this partial covariance is still not guaran-
 552 teed, it needs to be approximated to the nearest symmetric posi-
 553 tive semi-definite matrix when necessary (Higham, 1988). We can
 554 show, however, that this partial covariance is asymptotically posi-
 555 tive semi-definite in the small lapse limit (Appendix A),

556 **Infomax with MCMC.** Sampling-based inference provides an
 557 attractive alternative to Laplace’s method when the model includes
 558 non-zero lapse rates, where the posterior may be less well approx-
 559 imated by a Gaussian. To compute mutual information from sam-
 560 ples, it is more convenient to use the expansion given in (eq. 15), so
 561 that it is expressed as the expected uncertainty reduction in entropy
 562 of the response \mathbf{y} , instead of a reduction in the posterior entropy.

This will make it straightforward to approximate integrals needed
 for mutual information by Monte Carlo integrals involving sums
 over samples.

Given a set of set of posterior samples $\{\boldsymbol{\theta}_m\}$ from $p(\boldsymbol{\theta}|\mathcal{D}_t)$, the
 posterior distribution at time t , we can evaluate the mutual infor-
 mation using sums over “potential” terms that we denote by

$$L_{jm}(\mathbf{x}) \equiv p(y_j = 1|\mathbf{x}, \boldsymbol{\theta}_m). \quad (21)$$

This allows us to evaluate the conditional response entropy as

$$H_t(\mathbf{y}|\boldsymbol{\theta}; \mathbf{x}) \approx -\frac{1}{M} \sum_{j,m} L_{jm}(\mathbf{x}) \log L_{jm}(\mathbf{x}), \quad (22)$$

and the marginal response entropy as

$$H_t(\mathbf{y}; \mathbf{x}) \approx -\sum_j \left(\frac{1}{M} \sum_m L_{jm}(\mathbf{x}) \right) \log \left(\frac{1}{M} \sum_m L_{jm}(\mathbf{x}) \right), \quad (23)$$

where we have evaluated the posterior-predictive distribution as

$$p(y_j = 1|\mathbf{x}, \mathcal{D}_t) \approx \frac{1}{M} \sum_m L_{jm}(\mathbf{x}). \quad (24)$$

Putting together these terms, the mutual information can be evalu-
 ated as

$$I_t(\boldsymbol{\theta}; \mathbf{y}|\mathbf{x}) = -\frac{1}{M} \sum_{j,m} L_{jm}(\mathbf{x}) \log \frac{L_{jm}(\mathbf{x})}{\sum_{m'} L_{jm'}(\mathbf{x})/M}, \quad (25)$$

579 which is straightforward to evaluate for a set of candidate stimuli
580 $\{\mathbf{x}\}$. The computational cost of this approach is therefore linear
581 in the number of samples, and the primary concern is the cost of
582 obtaining a representative sample from the posterior.

583 Results

584 We consider two approaches for testing the performance of our pro-
585 posed stimulus-selection algorithms, one using simulated data, and
586 a second using an offline analysis of data from real psychophysical
587 experiments.

588 **Simulated experiments.** We first tested the performance of
589 our algorithms using simulated data from a fixed psychophysical
590 observer model. In these simulations, a stimulus \mathbf{x} was selected on
591 each trial and the observer’s response \mathbf{y} was sampled from a “true”
592 psychometric function, $p_{\text{true}}(\mathbf{y}|\mathbf{x}) = p(\mathbf{y}|\mathbf{x}, \boldsymbol{\theta}_{\text{true}})$.

593 We considered psychophysical models defined on a continuous
594 2-dimensional stimulus space with 4 discrete response alternatives
595 for every trial, corresponding to the problem of estimating the di-
596 rection of 2D stimulus moving along one of the four cardinal di-
597 rections (up, down, left, right). We computed expected informa-
598 tion gain over a set of discrete stimulus values corresponding to
599 21×21 square grid (Fig. 4A). The stimulus plane is colored in
600 Fig. 4A, to indicate the most likely response (one of the four alter-
601 natives) in each stimulus region. Lapse probabilities λ_{c_i} were set
602 to either zero (the “lapse-free” case), or a constant value of 0.05,
603 resulting in a total lapse probability of $\lambda = 0.2$ across the four
604 choices (Fig. 4B). We compared performance of our adaptive algo-
605 rithms with a method that selected a stimulus uniformly at random
606 from the grid on each trial. We observed that the adaptive methods
607 tended to sample more stimuli near the boundaries between colored
608 regions on the stimulus space (Fig. 4C), which led to more efficient
609 estimates of the PF compared to the uniform stimulus selection ap-
610 proach (Fig. 4D).

611 For each true model, we compared the performances of four dif-
612 ferent adaptive methods (Fig. 4E-F), defined by performing infer-

ence with MAP or MCMC, and assuming lapse rate to be fixed 613
at zero or including a non-zero lapse parameters. Each of these 614
inference methods was also applied to data selected according to 615
a uniform stimulus selection algorithm. We quantified perfor- 616
mance using the mean-squared error (MSE) between the true re- 617
sponse probabilities $p_{ij} = p(y = j|\mathbf{x}_i, \boldsymbol{\theta}_{\text{true}})$ and the estimated 618
probabilities \hat{p}_{ij} over the 21×21 grid of stimulus locations $\{\mathbf{x}_i\}$ 619
and the 4 possible responses $\{j\}$. For MAP-based inference, es- 620
timated probabilities were given by $\hat{p}_{ij} = p(y = j|\mathbf{x}_i, \hat{\boldsymbol{\theta}}_{\text{MAP}})$. 621
For the MCMC-based inference, probabilities were given by the 622
predictive distribution, evaluated using an average over samples: 623
 $\hat{p}_{ij} = \frac{1}{M} \sum_m p(y = j|\mathbf{x}_i, \boldsymbol{\theta}_m)$, where $\{\boldsymbol{\theta}_m\}$ represent samples 624
from the posterior. 625

When the true model was lapse-free (Fig. 4E), lapse-free and 626
lapse-aware inference methods performed similarly, indicating that 627
there was minimal cost to incorporating parameters governing 628
lapse when lapses were absent. Under all inference methods, in- 629
fomax stimulus selection outperformed uniform stimulus selec- 630
tion by a substantial margin. For example, infomax algorithms 631
achieved in 50 – 60 trials the error levels that their uniform- 632
stimulus-selection counterparts required 100 trials to achieve. 633

By contrast, when the true model had a non-zero lapse rate 634
(Fig. 4F), adaptive stimulus selection algorithms based on the 635
lapse-free model failed to select optimal stimuli, performing even 636
worse than uniform stimulus selection algorithms. This empha- 637
sizes the impact of model mismatch in adaptive methods, and the 638
importance of a realistic psychometric model. When lapse-aware 639
models were used for inference, on the other hand, both Laplace- 640
based and MCMC-based adaptive stimulus selection algorithms 641
achieved a significant speedup compared to uniform stimulus se- 642
lection, while MCMC-based adaptive algorithm performed bet- 643
ter. This shows that the MCMC-based infomax stimulus selection 644
method can provide an efficient and robust platform for adaptive 645
experiments with realistic models. 646

In view of these results, it seems good practice to always use the 647
lapse-aware model, unless the behavior under study is known to be 648

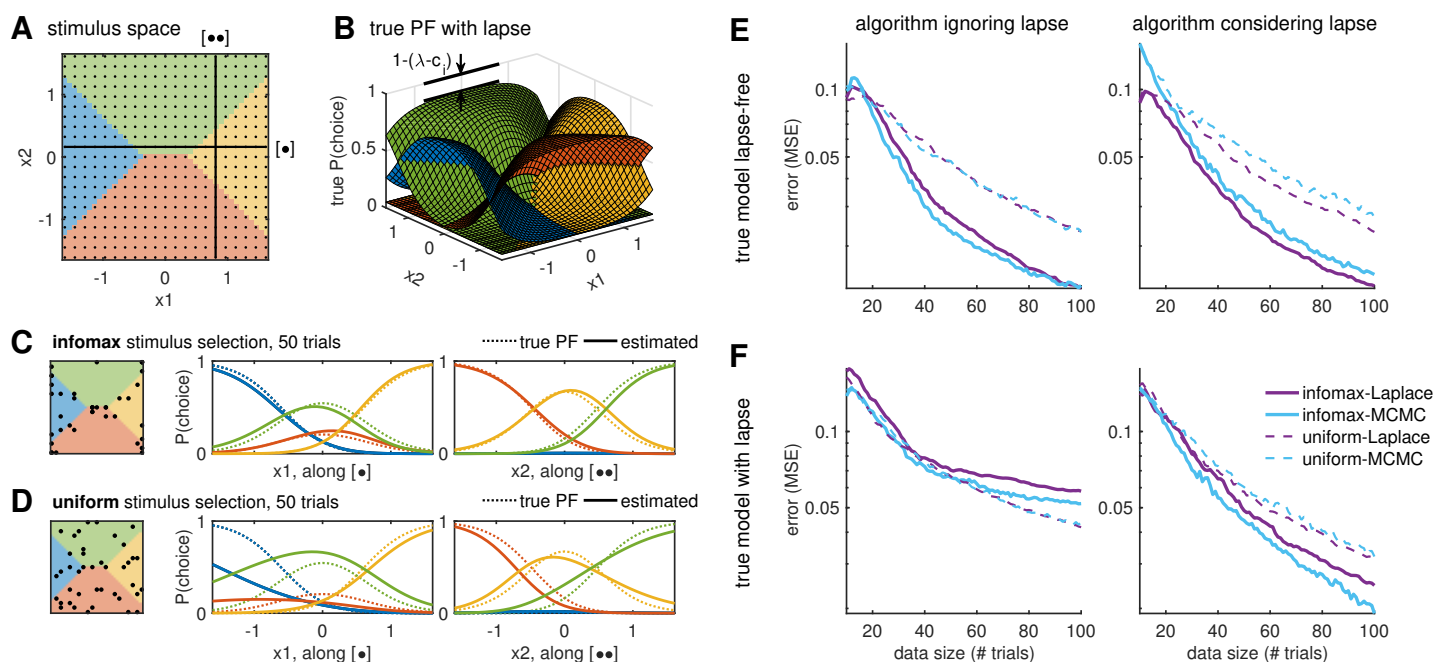


Figure 4: The simulated experiment. (A) At each trial, a stimulus was selected from a 2D stimulus plane with a 21×21 grid. The two lines, running along x_1 and x_2 respectively, indicate the cross-sections used in C and D below. Colors indicate the most likely response in the respective stimulus regime, according to the true PF shown in B, with a consistent color code. (B) Given each stimulus, a simulated response was drawn from a true model with 4 alternatives. Shown here is the model with lapse, characterized by a non-deterministic choice (i.e., the choice probability does not approach 0 or 1) even at an easy stimulus, far from the choice boundaries. (C-D) Examples of Laplace-approximation-based inference results after 50 trials, where stimuli was selected either using our adaptive infomax method (C) or uniformly (D), as shown on left. In both cases, the true model was lapse-free, and the algorithm assumed that lapse was fixed at zero. The two sets of curves show the cross-sections of the true PF (dotted lines) and the estimated PF (solid lines), along the two lines marked in A, after sampling these stimuli. (E-F) Error traces from simulated experiments, averaged over 100 runs each. The true model for simulation was either (E) lapse-free, or (F) with a finite lapse rate of $\lambda = 0.2$, with a uniform lapse scenario $c_i = 1/4$ for each outcome $i = 1, 2, 3, 4$. The algorithm either used the classical MNL model that assumes zero lapse (left column), or our extended model that considers lapse (right column). Performances of adaptive and uniform stimulus selection algorithms are plotted in solid and dashed lines; Laplace-based and MCMC-based algorithms are plotted in purple and cyan. All sampling-based algorithms used the semi-adaptive MCMC with chain length $M = 1000$.

649 completely lapse-free. The computational cost for incorporating
650 lapses amounts to having k additional parameters to sample, one
651 per each available choice, which is independent from the dimen-
652 sionality of the stimulus space. When the true behavior had lapses,
653 the MCMC-based adaptive stimulus selection algorithm with the
654 lapse-aware model automatically included “easy” trials, which pro-
655 vide maximal information about lapse probabilities. These easy
656 trials are typically in the periphery of the stimulus space (strong-
657 stimulus regimes, referred to as “asymptotic performance inten-
658 sity” in Prins (2012)).

659 **Optimal re-ordering of real dataset.** A second approach for
660 testing the performance of our methods is to perform an off-line
661 analysis of data from real psychophysical experiments. Here we
662 take an existing dataset and use our methods to re-order the trials
663 so that the most-informative stimuli are selected first. To obtain a
664 re-ordering, we iteratively apply our algorithm to the stimuli shown
665 during the experiment. On each trial, we use our adaptive algo-
666 rithm to select the optimal stimulus from the set of stimuli $\{\mathbf{x}_i\}$ not
667 yet incorporated into the model. This selection takes place without
668 access to the actual responses $\{y_i\}$. We then update the posterior
669 using the stimulus \mathbf{x}_i and the response y_i it actually elicited dur-
670 ing the experiment, then proceed to the next trial. We can then
671 ask whether adding the data according to the proposed re-ordering
672 would have led to faster narrowing of the posterior distribution than
673 other orderings.

674 To perform this analysis, we used a dataset from macaque
675 monkeys performing a four-alternative motion discrimination task
676 (Churchland, Kiani, & Shadlen, 2008). Monkeys were trained to
677 observe a motion stimulus with dots moving in one of the four car-
678 dinal directions, and report this direction of motion with an eye
679 movement. The difficulty of the task was controlled by varying the
680 fraction of coherently moving dots on each trial, with the remain-
681 ing dots appearing randomly (Fig. 5A). Each moving-dot stimulus
682 in this experiment could be represented as a two-dimensional vec-
683 tor, where the direction of the vector is the direction of the mean
684 movement of the dots, and the amplitude of the vector is given by

the fraction of coherently moving dots (a number between 0 and 685
1). Each stimulus presented in the the experiment was aligned with 686
either one of the two cardinal axes of the stimulus plane (Fig. 5B). 687
The PF for this dataset consists of a set of four 2D curves, where 688
each curve specifies the probability of choosing a particular direc- 689
tion as a function of location in the 2D stimulus plane (Fig. 5C). 690

This monkey dataset contained more than 10,000 total obser- 691
vations at 29 distinct stimulus conditions, accumulating more than 692
300 observations per stimulus. This multiplicity of observations 693
per stimulus ensured that the posterior distribution given the full 694
dataset was narrow enough that it could be considered to provide a 695
“ground truth” psychometric function against which the inferences 696
based on the re-ordering experiment could be compared. 697

The first 100 stimuli selected by the infomax algorithms had 698
noticeably different statistics than the full dataset or its uniform 699
sub-sampling (the first $N = 100$ trials under uniform sampling). 700
On the other hand, the sets of stimuli selected by both MAP- 701
based and MCMC-based infomax algorithms were similar. Fig. 5D 702
shows the histogram of stimulus component along one of the axes, 703
 $p(x_2 | x_1 = 0)$, from the first $N = 100$ trials, averaged over 100 704
independent runs under each stimulus selection algorithm using the 705
lapse-free model. 706

Because the true PF was unknown, we compared the perfor- 707
mance of each algorithm to an estimate of the PF from the entire 708
dataset. When using the MAP algorithm, the full-dataset PF was 709
given by $p_{ij} = p(y = j | \mathbf{x}_i, \hat{\theta}_{\text{full}})$, evaluated at the MAP estimate 710
of the log posterior, $\hat{\theta}_{\text{full}} = \text{argmax}_{\theta} \log p(\theta | \mathcal{D}_{\text{full}})$, given the full 711
dataset $\mathcal{D}_{\text{full}}$. For the MCMC algorithm, the full-dataset PF was 712
computed by $p_{ij} \approx \frac{1}{M} \sum_m p(y = j | \mathbf{x}_i, \theta_m)$, where the MCMC 713
chain $\{\theta_m\} \sim \log p(\theta | \mathcal{D}_{\text{full}})$ sampled the log posterior given the 714
full dataset. The re-ordering test on the monkey dataset showed 715
that our adaptive stimulus sampling algorithms were able to infer 716
the PF to a given accuracy in a smaller number of observations, 717
compared to a uniform sampling algorithm (Fig. 5E-F). In other 718
words, data collection could have been faster with an optimal re- 719
ordering of the experimental procedure. 720

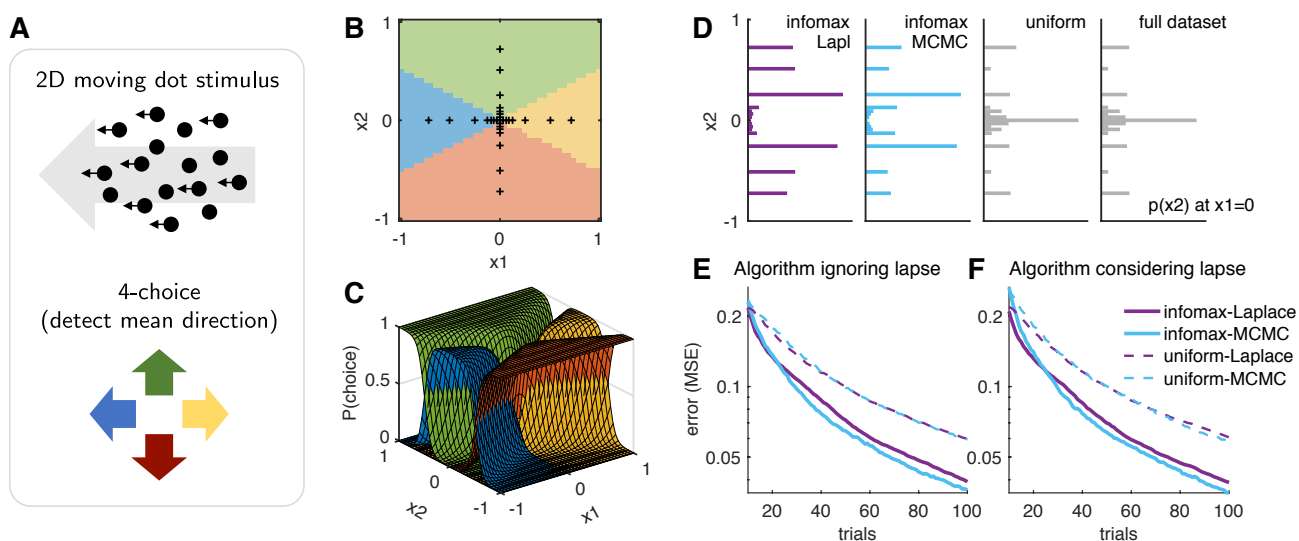


Figure 5: Optimal re-ordering of a real monkey dataset. (A) The psychometric task consisted of a 2D stimulus presented as moving dots, characterized by a coherence and a mean direction of movement, and a 4-alternative response. The four choices are color coded consistently in A-C in this figure. (B) The axes-only stimulus space of the original dataset, with 15 fixed stimuli along each axis. Colors indicate the most likely response in the respective stimulus regime according to the best estimate of the PF. (C) The best estimate of the PF of monkeys in this task, inferred from all observations in the dataset. (D) Stimuli selection in the first $N = 100$ trials during the re-ordering experiment, under the inference method that ignores lapse. Shown are histograms of x_2 along one of the axes, $x_1 = 0$, averaged over 100 independent runs in each case. (E-F) Error traces under different algorithms, averaged over 100 runs. Both Laplace-based (purple) and MCMC-based (cyan; with $M = 1000$) algorithms achieve significant speedups over uniform sampling. Because the monkeys were almost lapse-free in this task, inference methods that ignore lapse (E) and consider lapse (F) performed similarly.

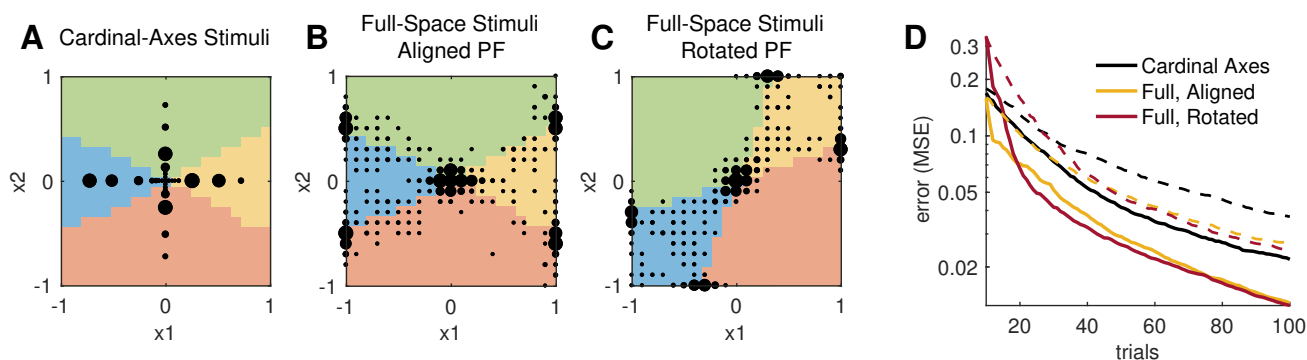


Figure 6: Design of multi-dimensional stimulus space. (A-C) Three different stimulus space designs were used in a simulated psychometric experiment. Responses were simulated according to fixed lapse-free PFs, matched to our best estimate of the monkey PF (Fig. 5C). Stimuli were selected within the respective stimulus spaces, (A) the cardinal-axes design, as in the original experiment; (B) full stimulus plane, with the PF aligned to the cardinal axes of the original stimulus space; (C) full stimulus plane, with rotated PF. The black dots in A-C indicate which stimuli were sampled by the Laplace-based infomax algorithm during the first $N = 100$ trials of simulation, where the dot size is proportional to the number of trials in which each stimulus was selected (averaged over 20 independent runs, and excluding the 10 fixed initial stimuli). (D) The corresponding error traces, under infomax (solid lines) or uniform (dashed lines) stimulus selection, averaged over 100 runs respectively. Colors indicate the three stimulus space designs, as shown in A-C.

721 **Exploiting the full stimulus space.** In the experimental
722 dataset considered in the previous section, the motion stimuli were
723 restricted to points along the cardinal axes of the 2D stimulus plane
724 (Fig. 5B) (Churchland et al., 2008). In some experimental settings,
725 however, the psychometric functions of interest may lack identi-
726 fiable axes of alignment or may exhibit asymmetries in shape or
727 orientation. Here we show that in such cases, adaptive stimulus
728 selection methods can benefit from the ability to select points from
729 the full space of possible stimuli.

730 We performed experiments with a simulated observer gov-
731 erned by the lapse-free psychometric function estimated from the
732 macaque monkey dataset (Fig. 5C). This psychometric function
733 was either aligned to the original stimulus axes (Fig. 6A-B) or ro-
734 tated counter-clockwise by 45 degrees (Fig. 6C). We tested the per-
735 formance of adaptive stimulus selection using the Laplace infomax
736 algorithm, with stimuli restricted to points along the cardinal axes
737 (Fig. 6A), or allowed to a grid of points in the full 2D stimulus
738 plane (Fig. 6B-C).

739 The simulated experiment indeed closely resembled the results
740 of our dataset re-ordering test in terms of the statistics of adap-
741 tively selected stimuli (compare Fig. 6A to the purple histogram in
742 Fig. 5D). With the full 2D stimulus space aligned to the cardinal
743 axes, on the other hand, our adaptive infomax algorithm detected
744 and sampled more stimuli near the boundaries between colored re-
745 gions in the stimulus plane, which were usually not on the cardi-
746 nal axes (Fig. 6B). Finally, we also observed that this automatic
747 exploitation of the stimulus space was not limited by the lack of
748 alignment between the PF and the stimulus axes; our adaptive in-
749 fomax algorithm was just as effective in detecting and sampling the
750 boundaries between stimulus regions in the case of the unaligned
751 PF (Fig. 6C).

752 The error traces in Fig. 6D show that we can infer the PF at a
753 given accuracy in an even fewer number of observations using our
754 adaptive algorithm on the full 2D stimulus plane (orange curves),
755 compared to the cardinal-axes design (black curves). It also con-
756 firms that we can infer the PF accurately and effectively with an

unaligned stimulus space (red curves), as well as with an aligned
stimulus space. For comparison purposes, all errors were calcu-
lated over the same 2D stimulus grid, even when the stimulus se-
lection was from the cardinal axes. (This had negligible effects on
the resulting error values: compare the black curves in Fig. 6D and
the purple curves in Fig. 5E.)

763 Discussion

764 We developed effective Bayesian adaptive stimulus selection al-
765 gorithms for inferring psychometric functions, with an objective of
766 maximizing the expected informativeness of each stimulus. The al-
767 gorithms select an optimal stimulus adaptively in each trial, based
768 on the posterior distribution of model parameters inferred from the
769 accumulating set of past observations.

770 We emphasized that in psychometric experiments, especially
771 with animals, it is crucial to use models that can account for the
772 non-ideal yet common behaviors, such as omission (no response;
773 an additional possibility for the outcome) or lapse (resulting in
774 a random, stimulus-independent response). Specifically, we con-
775 structed a hierarchical extension of a multinomial logistic (MNL)
776 model that incorporates both omission and lapse. To ensure ap-
777 plicability of the extended model in real-time closed-loop adaptive
778 stimulus selection algorithms, we also developed efficient meth-
779 ods for inferring the posterior distribution of the model parameters,
780 with approximations specifically suited for sequential experiments.

781 **Advantages of adaptive stimulus selection.** We observed
782 two important advantages of using Bayesian adaptive stimulus se-
783 lection methods in psychometric experiments. First, we showed
784 that our adaptive stimulus selection algorithms achieved signifi-
785 cant speed-ups in learning time (number of measurements), both
786 on simulated data and in re-ordering test of a real experimental
787 dataset, with and without lapse in the underlying behavior. Import-
788 antly, the success of the algorithm depends heavily on the use of
789 the correct model family; for example, adaptive stimulus selection
790 fails when a classical (lapse-ignorant) model was used to measure

791 behavior with a finite lapse rate. Based on the simulation results,
792 it is always a good idea to use the our extended model which can
793 accommodate both lapse-free and finite-lapse systems.

794 Second, we demonstrated that our adaptive stimulus selection
795 study has implications on the optimization of the experimental de-
796 signs more generally. Contrary to the conventional practice of ac-
797 cumulating repeated observations at a small set of fixed stimuli, we
798 suggest that the (potentially high-dimensional) stimulus space can
799 be exploited more efficiently using our Bayesian adaptive stimulus
800 selection algorithm. Specifically, the adaptive stimulus selection
801 algorithm can automatically detect the structure of the stimulus
802 space (with respect to the psychometric function) as part of the
803 process. We also showed that there are benefits of using the full
804 stimulus space even when the PF is aligned to the cardinal axes of
805 the stimulus space.

806 **Comparison of the two algorithms.** Our adaptive stimulus
807 selection algorithms were developed based on two methods for ef-
808 fective posterior inference: one based on local Gaussian approxi-
809 mation (Laplace approximation) of the posterior, and another based
810 on MCMC sampling. Although the well-studied analytical method
811 based on the Laplace approximation is fast and effective in ideal
812 settings (where log concavity is guaranteed), it may break down
813 with a departure from the ideal model, for example with a finite
814 lapse rate. The sampling-based method is a robust alternative for
815 those realistic situations.

816 In the case of sampling-based methods, the cost of such flexi-
817 bility comes in the form of increased computation time; depending
818 on the experimental paradigm, a naive implementation of the sam-
819 pling method may take too long to run within a single-trial interval.
820 For real-time applications, therefore, it will be an important future
821 direction to further optimize the sampling algorithm. For example,
822 in this work, we developed a semi-adaptive tuning algorithm to ef-
823 ficiently transfer step-size information from the previous trials to
824 the current trial. On the other hand, the computational bottleneck
825 for the Laplace-approximation-based method in this work was the
826 high-dimensional integration in the infomax calculation; a more

accurate estimate would require the quadrature to be on a finer grid
of support points.

Adaptive designs in psychometric experiments. Finally,
we note that a potential limitation of the adaptive stimulus selec-
tion framework is the (undesired) possibility that the psychometric
function of the observer might adapt to the distribution of stimuli
presented during the experiments. If this is the case, the system un-
der measurement would no longer be stationary, nor independent
of the experimental design, profoundly altering the problem one
should try to solve.

The usual assumption in psychometric experiments is that, al-
though behavior adaptation is the major process in the training
phase (Bak, Choi, Akrami, Witten, & Pillow, 2016), already over-
trained observers would not change their behavior too quickly, par-
ticularly not within the timescale of a psychometric experiment.
Under such assumption of stationarity, as pointed out by MacKay
(1992), the order of data collection cannot bias the Bayesian infer-
ence.

In order to justify the use of adaptive designs, the impact of
post-training adaptation will need to be tested experimentally. For
example, it was suggested that the inter-trial dependence was
non-negligible even in overtrained animals (Fründ, Wichmann, &
Macke, 2014); there have been attempts to account for the history
dependence by adding regressors on relevant features in a small
number of preceding trials, such as the reward outcomes (Bak et
al., 2016; Busse et al., 2011; Corrado, Sugrue, Seung, & Newsome,
2005; Lau & Glimcher, 2005), the stimuli (Akrami, Kopec, Dia-
mond, & Brody, 2017) or the full stimulus-response history (Fründ
et al., 2014). Whether the adaptive stimulus presentation can have
more systematic impacts, on the behavior of trained observers, re-
mains an open question.

Acknowledgements

We thank Anne Churchland for sharing the monkey data. JHB was
supported by the Samsung Scholarship for the study at Princeton.

861 JWP was supported by grants from the McKnight Foundation, Si-
862 mons Collaboration on the Global Brain (SCGB AWD1004351)
863 and the NSF CAREER Award (IIS-1150186). Computational work
864 was performed using resources at Princeton University and the
865 KIAS Center for Advanced Computing.

Chaloner, K., & Verdinelli, I. (1995). Bayesian experimental de- 894
sign: a review. *Statistical Science*, *10*, 273–304. 895

Churchland, A. K., Kiani, R., & Shadlen, M. N. (2008). Decision- 896
making with multiple alternatives. *Nature Neuroscience*, 897
11(6), 693–702. doi: 10.1038/nn.2123 898

Corrado, G. S., Sugrue, L. P., Seung, H. S., & Newsome, W. T. 899
(2005). Linear-nonlinear-poisson models of primate choice 900
dynamics. *Journal of the Experimental Analysis of Behavior*, 901
84(3), 581–617. doi: 10.1901/jeab.2005.23-05 902

DiMattina, C. (2015). Fast adaptive estimation of multidimen- 903
sional psychometric functions. *Journal of Vision*, *15*(9), 5. 904
doi: 10.1167/15.9.5 905

DiMattina, C., & Zhang, K. (2011). Active data collection 906
for efficient estimation and comparison of nonlinear neu- 907
ral models. *Neural Computation*, *23*(9), 2242–2288. doi: 908
10.1162/NECO_a.00167 909

Fründ, I., Wichmann, F. A., & Macke, J. H. (2014). Quantifying 910
the effect of intertrial dependence on perceptual decisions. 911
Journal of vision, *14*(7), 1–16. doi: 10.1167/14.7.9 912

Gelman, A., Roberts, G., & Gilks, W. (1996). Efficient metropolis 913
jumping rules. *Bayesian statistics*, *5*, 599–607. 914

Glonek, G., & McCullagh, P. (1995). Multivariate Logistic 915
Models. *Journal of the Royal Statistical Society, Series B* 916
(*Methodological*), *57*(3), 533–546. 917

Haario, H., Saksman, E., & Tamminen, J. (2001). An adaptive 918
metropolis algorithm. *Bernoulli*, *7*(2), 223–242. doi: 10 919
.2307/3318737 920

Heiss, F., & Winschel, V. (2008). Likelihood approximation by 921
numerical integration on sparse grids. *Journal of Economet-* 922
rics, *144*(1), 62–80. doi: 10.1016/j.jeconom.2007.12.004 923

Henderson, H. V., & Searle, S. R. (1981). On deriving the inverse 924
of a sum of matrices. *SIAM Review*, *23*(1), 53–60. doi: 925
10.1137/1023004 926

Higham, N. J. (1988). Computing a nearest symmetric positive 927

866 References

867 Akrami, A., Kopec, C. D., Diamond, M. E., & Brody, C. D. (2017).
868 Posterior parietal cortex represents sensory stimulus history
869 and is necessary for its effects on behavior. *bioRxiv*. doi:
870 10.1101/182246

871 Bak, J. H., Choi, J. Y., Akrami, A., Witten, I. B., & Pillow, J. W.
872 (2016). Adaptive optimal training of animal behavior. In
873 *Advances in neural information processing systems* *29* (pp.
874 1947–1955).

875 Bishop, C. M. (2006). *Pattern recognition and machine learning*.
876 Springer New York.

877 Busse, L., Ayaz, A., Dhruv, N. T., Katzner, S., Saleem, A. B.,
878 Scholvinck, M. L., ... Carandini, M. (2011). The de-
879 tection of visual contrast in the behaving mouse. *Jour-*
880 *nal of Neuroscience*, *31*(31), 11351–11361. doi: 10.1523/
881 JNEUROSCI.6689-10.2011

882 Carandini, M., & Churchland, A. K. (2013). Probing perceptual
883 decisions in rodents. *Nature Neuroscience*, *16*(7), 824–831.
884 doi: 10.1038/nn.3410

885 Cavagnaro, D. R., Myung, J. I., Pitt, M. A., & Kujala, J. V. (2010).
886 Adaptive design optimization: a mutual information-based
887 approach to model discrimination in cognitive science. *Neu-*
888 *ral computation*, *22*(4), 887–905. doi: 10.1162/neco.2009
889 .02-09-959

890 Chaloner, K., & Larntz, K. (1989). Optimal logistic Bayesian
891 design applied to logistic regression experiments. *Journal*
892 *of Statistical Planning and Inference*, *21*, 191–208. doi: 10
893 .1016/0378-3758(89)90004-9

- 928 semidefinite matrix. *Linear Algebra and Its Applications*,
929 103(C), 103–118. doi: 10.1016/0024-3795(88)90223-6
- 930 Kim, W., Pitt, M. A., Lu, Z.-l., Steyvers, M., & Myung, J. I.
931 (2014). A hierarchical adaptive approach to optimal ex-
932 perimental design paradigm of adaptive design optimiza-
933 tion (ADO). *Neural computation*, 26, 2465–2492. doi:
934 10.1162/NECO_a.00654
- 935 Knoblauch, K., & Maloney, L. T. (2008). Estimating classification
936 images with generalized linear and additive models. *Journal*
937 *of Vision*, 8(16), 10.1–1019. doi: 10.1167/8.16.10
- 938 Kontsevich, L. L., & Tyler, C. W. (1999). Bayesian adaptive es-
939 timation of psychometric slope and threshold. *Vision Re-*
940 *search*, 39(16), 2729–2737. doi: 10.1016/S0042-6989(98)
941 00285-5
- 942 Kujala, J. V., & Lukka, T. J. (2006). Bayesian adaptive estimation:
943 The next dimension. *Journal of Mathematical Psychology*,
944 50(4), 369–389. doi: 10.1016/j.jmp.2005.12.005
- 945 Kuss, M., Jäkel, F., & Wichmann, F. A. (2005). Bayesian inference
946 for psychometric functions. *Journal of Vision*, 5(5), 478–
947 492. doi: 10.1167/5.5.8
- 948 Lau, B., & Glimcher, P. W. (2005). Dynamic response-by-response
949 models of matching behavior in rhesus monkeys. *Journal of*
950 *the Experimental Analysis of Behavior*, 84(3), 555–579. doi:
951 10.1901/jeab.2005.110-04
- 952 Lesmes, L. A., Lu, Z.-L., Baek, J., & Albright, T. D. (2010).
953 Bayesian adaptive estimation of the contrast sensitivity func-
954 tion: the quick CSF method. *Journal of Vision*, 10(3), 17.1–
955 21. doi: 10.1167/10.3.17
- 956 Lewi, J., Butera, R., & Paninski, L. (2009). Sequential optimal de-
957 sign of neurophysiology experiments. *Neural computation*,
958 21(3), 619–687. doi: 10.1162/neco.2008.08-07-594
- 959 MacKay, D. J. C. (1992). Information-based objective functions
960 for active data selection. *Neural Computation*, 4(4), 590–
961 604. doi: 10.1162/neco.1992.4.4.590
- Metropolis, N., Rosenbluth, A. W., Rosenbluth, M. N., Teller,
962 A. H., & Teller, E. (1953). Equation of state calculations by
963 fast computing machines. *The Journal of Chemical Physics*,
964 21(6), 1087. doi: 10.1063/1.1699114
- Murray, R. F. (2011). Classification images: A review. *Journal of*
966 *Vision*, 11(5). doi: 10.1167/11.5.2
- Neri, P., & Heeger, D. J. (2002). Spatiotemporal mechanisms for
968 detecting and identifying image features in human vision.
969 *Nat Neurosci*, 5(8), 812–816. doi: 10.1038/nn886
- Paninski, L., Ahmadian, Y., Ferreira, D. G., Koyama, S., Rah-
971 nama Rad, K., Vidne, M., ... Wu, W. (2010). A new
972 look at state-space models for neural data. *Journal of Com-*
973 *putational Neuroscience*, 29(1), 107–126. doi: 10.1007/
974 s10827-009-0179-x
- Park, M., Horwitz, G., & Pillow, J. W. (2011). Active learning
976 of neural response functions with Gaussian processes. In
977 *Advances in neural information processing systems 24* (pp.
978 2043–2051). 979
- Park, M., & Pillow, J. W. (2012). Bayesian active learning with
980 localized priors for fast receptive field characterization. In
981 *Advances in neural information processing systems 25* (pp.
982 2357–2365). 983
- Park, M., Weller, J. P., Horwitz, G. D., & Pillow, J. W. (2014).
984 Bayesian active learning of neural firing rate maps with
985 transformed Gaussian process priors. *Neural Computation*,
986 26, 1519–1541. doi: 10.1162/NECO_a.00615
- Pillow, J. W., Ahmadian, Y., & Paninski, L. (2011). Model-based
988 decoding, information estimation, and change-point detec-
989 tion techniques for multineuron spike trains. *Neural Com-*
990 *putation*, 23(1), 1–45. doi: 10.1162/NECO_a.00058
- Pillow, J. W., & Park, M. (2016). Adaptive Bayesian methods for
992 closed-loop neurophysiology. In A. E. Hady (Ed.), *Closed*
993 *loop neuroscience*. Elsevier. 994
- Prins, N. (2012). The psychometric function: The lapse rate revis-
995 ited. *Journal of Vision*, 12(6), 25–25. doi: 10.1167/12.6.25 996

997 Prins, N. (2013). The psi-marginal adaptive method: How to give
 998 nuisance parameters the attention they deserve (no more, no
 999 less). *Journal of Vision*, 13(7), 1–17. doi: 10.1167/13.7.3

1000 Roberts, G. O., Gelman, A., & Gilks, W. R. (1997). Weak conver-
 1001 gence and optimal scaling of random walk Metropolis algo-
 1002 rithms. *Annals of Applied Probability*, 7(1), 110–120. doi:
 1003 10.1214/aoap/1034625254

1004 Rosenthal, J. S. (2011). Optimal proposal distributions and adap-
 1005 tive mcmc. In S. Brooks, A. Gelman, G. Jones, & X.-
 1006 L. Meng (Eds.), *Handbook of Markov Chain Monte Carlo*
 1007 (pp. 93–112). Chapman and Hall CRC. doi: 10.1201/
 1008 b10905

1009 Watson, A. B. (2017). QUEST+: A general multidimensional
 1010 Bayesian adaptive psychometric method. *Journal of Vision*,
 1011 17(3), 10. doi: 10.1167/17.3.10

1012 Watson, A. B., & Pelli, D. G. (1983). QUEST: A Bayesian adaptive
 1013 psychometric method. *Perception & psychophysics*, 33(2),
 1014 113–120. doi: 10.3758/BF03202828

1015 Wichmann, F. A., & Hill, N. J. (2001). The psychometric function:
 1016 I. Fitting, sampling, and goodness of fit. *Perception & psy-
 1017 chophysics*, 63(8), 1293–1313. doi: 10.3758/BF03194544

1018 Zocchi, S. S., & Atkinson, A. C. (1999). Optimum experimental
 1019 designs for multinomial logistic models. *Biometrics*, 55(2),
 1020 437–444. doi: 10.1111/j.0006-341X.1999.00437.x

Appendix A

Log likelihood for the classical MNL. Here we provide more
 details about the log likelihood $L = \mathbf{y}^\top \log \mathbf{p}$ under the multino-
 mial logistic model (6), first in the lapse-free case.

A convenient property of the multinomial logistic model (a prop-
 erty common to all generalized linear models) is that the parameter
 vector p_i governing y depends only on a 1-dimensional projection
 of the input, $V_i = \phi^\top \mathbf{w}_i$, which is known as the *linear predictor*.
 Recall that $\phi = \phi(\mathbf{x})$ is the input feature vector. In the multinomial
 case, it is useful to consider the column vector of linear predictors
 for a single trial, $\mathbf{V} = [V_1, \dots, V_k]^\top$, and the concatenated weight
 vector $\mathbf{w} = [\mathbf{w}_1^\top, \dots, \mathbf{w}_k^\top]^\top$, consisting of all weights stacked
 into a single vector. We can summarize their linear relationship
 as $\mathbf{V} = X\mathbf{w}$, where X is a block diagonal matrix containing k
 blocks of ϕ^\top along the diagonal. In other words,

$$X = \begin{bmatrix} \phi^\top & \mathbf{0}^\top & \dots & \mathbf{0}^\top \\ \mathbf{0}^\top & \phi^\top & \dots & \mathbf{0}^\top \\ \vdots & \vdots & \ddots & \vdots \\ \mathbf{0}^\top & \mathbf{0}^\top & \dots & \phi^\top \end{bmatrix}, \quad \mathbf{w} = \begin{bmatrix} \mathbf{w}_1 \\ \mathbf{w}_2 \\ \vdots \\ \mathbf{w}_k \end{bmatrix}. \quad (26)$$

Derivatives. It is convenient to work in terms of the linear pre-
 dictor $\mathbf{V} = \{V_i\}$ first. If $N_y \equiv \sum_i y_i = 1$ is the total number of
 responses per trial, the first and second derivatives of L with respect
 to \mathbf{V} are $\partial L / \partial V_j = y_j - N_y p_j$ and $\partial^2 L / \partial V_i \partial V_j = N_y p_i (\delta_{ij} - p_j)$,
 respectively. Rewriting in vector forms, we have

$$\frac{\partial L}{\partial \mathbf{V}} = (\mathbf{y} - N_y \mathbf{p})^\top, \quad (27)$$

$$\frac{\partial^2 L}{\partial \mathbf{V}^2} = -N_y (\text{diag}(\mathbf{p}) - \mathbf{p}\mathbf{p}^\top) \equiv -N_y \Gamma(\mathbf{p}), \quad (28)$$

where $\text{diag}(\mathbf{p}) = [p_i \delta_{ij}]$ is a square matrix with the elements of \mathbf{p}
 on the diagonal, and zeros otherwise.

Putting back in terms of the weight vector \mathbf{w} is easy, thanks to
 the linear relationship $\mathbf{V} = X\mathbf{w}$:

$$\frac{\partial L}{\partial \mathbf{w}} = \frac{\partial L}{\partial \mathbf{V}} X = (\mathbf{y} - \mathbf{p})^\top X \equiv \mathbf{\Delta}^\top, \quad (29)$$

$$\frac{\partial^2 L}{\partial \mathbf{w}^2} = X^\top \frac{\partial^2 L}{\partial \mathbf{V}^2} X = -X^\top \Gamma X \equiv -\Lambda. \quad (30)$$

1052 **Concavity.** Importantly, L is concave with respect to \mathbf{V} (and
1053 therefore with respect to \mathbf{w}). To prove the concavity of L , we
1054 show that the Hessian $H = -\text{diag}(\mathbf{p}) + \mathbf{p}\mathbf{p}^\top \equiv -\Gamma$ is nega-
1055 tive semi-definite, which is equivalent to showing that $\mathbf{z}^\top \Gamma \mathbf{z} \geq 0$
1056 for an arbitrary vector \mathbf{z} .

$$\begin{aligned} \mathbf{z}^\top \Gamma \mathbf{z} &= \mathbf{z}^\top \text{diag}(\mathbf{p}) \mathbf{z} - (\mathbf{z}^\top \mathbf{p})^2 \\ &= \sum_i z_i^2 p_i - \left(\sum_j z_j p_j \right)^2 \\ &= \sum_i z_i^2 p_i - 2 \sum_i z_i p_i \sum_j z_j p_j + \left(\sum_j z_j p_j \right)^2 \\ &= \sum_i p_i \left[z_i^2 - 2 z_i \sum_j z_j p_j + \left(\sum_j z_j p_j \right)^2 \right] \\ &= \sum_i p_i \left[\left(z_i - \sum_j z_j p_j \right)^2 \right] \geq 0. \end{aligned} \quad (31)$$

1064 **Log likelihood with lapse.** With a finite lapse rate λ , to recap,
1065 the multinomial logistic model is modified as $p_i = (1 - \lambda)q_i + \lambda c_i$
1066 where

$$q_i = \frac{\exp(V_i)}{\sum_j \exp(V_j)}, \quad \lambda c_i = \frac{\exp(u_i)}{1 + \sum_j \exp(u_j)}. \quad (32)$$

1068 Let us introduce the following abbreviations,

$$r_i \equiv \frac{\lambda c_i}{p_i}, \quad t_i \equiv y_i(1 - r_i), \quad s_i \equiv y_i r_i(1 - r_i), \quad (33)$$

1070 where the dimensionless ratio $r \in [0, 1]$ can be considered as the
1071 order parameter for the effect of lapse.

1072 **Derivatives with respect to the weights.** Differentiating with the
1073 linear predictor \mathbf{V} , we get

$$\begin{aligned} \frac{\partial q_i}{\partial V_l} &= (\delta_{il} - q_l) q_i, \\ \frac{\partial^2 q_i}{\partial V_j \partial V_l} &= [(\delta_{ij} - q_j)(\delta_{il} - q_l) - (\delta_{jl} q_l - q_j q_l)] q_i. \end{aligned}$$

1077 which leads to

$$\frac{\partial p_i}{\partial V_l} = (1 - \lambda) \frac{\partial q_i}{\partial V_l}, \quad \frac{\partial^2 p_i}{\partial V_j \partial V_l} = (1 - \lambda) \frac{\partial^2 q_i}{\partial V_j \partial V_l}.$$

1079 We are interested in the derivatives of the log likelihood $L =$
1080 $\mathbf{y}^\top \log \mathbf{p}$ with respect to \mathbf{V} . The partial gradient:

$$\begin{aligned} \frac{\partial L}{\partial V_l} &= \sum_i y_i \frac{1}{p_i} \frac{\partial p_i}{\partial V_l} = (1 - \lambda) \sum_i y_i \frac{q_i}{p_i} (\delta_{il} - q_l) \\ &= t_l - q_l \sum_i t_i. \end{aligned}$$

Similarly, the partial Hessian is written as

$$\begin{aligned} \frac{\partial^2 L}{\partial V_j \partial V_l} &= \sum_i y_i \left(\frac{1}{p_i} \frac{\partial^2 p_i}{\partial V_j \partial V_l} - \frac{1}{p_i^2} \frac{\partial p_i}{\partial V_j} \frac{\partial p_i}{\partial V_l} \right) \\ &= \delta_{jl} (s_l - q_l \sum_i t_i) - (q_j s_l + q_l s_j) + q_j q_l (\sum_i s_i + \sum_i t_i). \end{aligned}$$

In vector forms, and with $\tau \equiv \sum_i t_i$ and $\sigma \equiv \sum_i s_i$,

$$\frac{\partial L}{\partial \mathbf{V}} = (\mathbf{t} - \tau \mathbf{q})^\top; \quad (34)$$

$$\begin{aligned} \frac{\partial^2 L}{\partial \mathbf{V}^2} &= \text{diag}(\mathbf{s} - \tau \mathbf{q}) - (\mathbf{q}\mathbf{s}^\top + \mathbf{s}\mathbf{q}^\top) + (\tau + \sigma) \mathbf{q}\mathbf{q}^\top \\ &= -\tau [\text{diag}(\mathbf{q}) - \mathbf{q}\mathbf{q}^\top] \\ &\quad + [\text{diag}(\mathbf{s}) - (\mathbf{q}\mathbf{s}^\top + \mathbf{s}\mathbf{q}^\top) + \sigma \mathbf{q}\mathbf{q}^\top]. \end{aligned} \quad (35)$$

Note that we recover $t_i \rightarrow y_i$ and $s_i \rightarrow 0$ in the lapse-free limit
 $\lambda \rightarrow 0$. Hence the first square bracket in (35) reduces back to
the lapse-free Hessian, while the second square bracket vanishes
as $\lambda \rightarrow 0$.

In the presence of lapse, one might still be interested in the
partial Hessian with respect to the weight parameters, $H \equiv$
 $\partial^2 L / \partial \mathbf{V}^2$, which should be evaluated as in (35). To test the nega-
tive semi-definiteness of this partial Hessian, again for an arbitrary
vector \mathbf{z} , we end up with

$$\mathbf{z}^\top H \mathbf{z} = - \sum_j t_j \left\langle (z - \langle z \rangle_q)^2 \right\rangle_q + \sum_j s_j \left(z_j - \langle z \rangle_q \right)^2 \quad (36)$$

where $\langle x \rangle_q = \sum_j x_j q_j$. The partial Hessian is asymptotically neg-
ative semi-definite (which is equivalent to the log likelihood being
concave) in the lapse-free limit, where $t_j \rightarrow y_j$ and $s_j \rightarrow 0$.

Derivatives with respect to lapse parameters. From (2) and (3),
we have $p_i = (1 - \lambda)q_i + \lambda c_i$ where

$$c_i = \frac{\exp(u_i)}{\sum_j \exp(u_j)}; \quad \lambda = \frac{\sum_j \exp(u_j)}{1 + \sum_j \exp(u_j)}. \quad (37)$$

Differentiating with respect to the auxiliary lapse parameter u_i ,

$$\frac{\partial c_i}{\partial u_j} = (\delta_{ij} - c_i) c_j; \quad \frac{\partial \lambda}{\partial u_j} = (1 - \lambda) \lambda c_j. \quad (38)$$

The gradient is then

$$\frac{\partial p_i}{\partial u_j} = (\delta_{ij} - p_i) \lambda c_j; \quad (39)$$

1117 using the abbreviations in (33), the gradient of the log likelihood is

$$\frac{\partial L}{\partial u_j} = \sum_i y_i \frac{1}{p_i} \frac{\partial p_i}{\partial u_j} = r_j (y_j - N_y \cdot p_j). \quad (40)$$

1120 Second derivative with respect to lapse:

$$\frac{\partial^2 p_i}{\partial u_j \partial u_l} = \delta_{jl} \frac{\partial p_i}{\partial u_l} - (\delta_{ij} + \delta_{il} - 2p_i) \lambda c_l \lambda c_j; \quad (41)$$

1123 it is useful to notice that

$$\frac{\partial p_i}{\partial u_j} \frac{\partial p_i}{\partial u_l} = \delta_{jl} \frac{\partial p_i}{\partial u_l} \lambda c_l - p_i (\delta_{ij} + \delta_{il} - 2p_i) \lambda c_l \lambda c_j. \quad (42)$$

1126 The corresponding part of the Hessian:

$$\begin{aligned} \frac{\partial^2 L}{\partial u_j \partial u_l} &= \sum_i y_i \left(\frac{1}{p_i} \frac{\partial^2 p_i}{\partial u_j \partial u_l} - \frac{1}{p_i^2} \frac{\partial p_i}{\partial u_j} \frac{\partial p_i}{\partial u_l} \right) \\ &= \delta_{jl} \sum_i y_i \frac{1}{p_i} \left(1 - \frac{\lambda c_l}{p_i} \right) \frac{\partial p_i}{\partial u_l} \\ &= \delta_{jl} \left(s_l - r_l p_l N_y + r_l^2 p_l^2 \sum_i \frac{y_i}{p_i} \right). \end{aligned} \quad (43)$$

1131 Finally, the mixed derivative:

$$\frac{\partial^2 p_i}{\partial u_j \partial V_l} = -(1 - \lambda) \lambda c_j \cdot (\delta_{il} - q_l) q_l. \quad (44)$$

1134 again it is useful to notice that

$$\frac{\partial p_i}{\partial u_j} \frac{\partial p_i}{\partial V_l} = -(\delta_{ij} - p_i) \frac{\partial^2 p_i}{\partial u_j \partial V_l}. \quad (45)$$

1137 Hence

$$\begin{aligned} \frac{\partial^2 L}{\partial u_j \partial V_l} &= \sum_i y_i \left(\frac{1}{p_i} \frac{\partial^2 p_i}{\partial u_j \partial V_l} - \frac{1}{p_i^2} \frac{\partial p_i}{\partial u_j} \frac{\partial p_i}{\partial V_l} \right) \\ &= -s_j \left(\delta_{jl} + \frac{q_l^2}{q_j} \right). \end{aligned} \quad (46)$$

1141 From (40), (43) and (46), we see that all derivatives involving the
1142 lapse parameter scale with at least one order of r , therefore vanish-
1143 ing in the lapse-free limit $\lambda \rightarrow 0$.

1144 Appendix B

1145 **The Metropolis-Hastings algorithm.** The Metropolis-
1146 Hastings algorithm (Metropolis et al., 1953) generates a chain of
1147 samples, using a proposal density and a method to accept or reject
1148 the proposed moves.

A proposal is made at each iteration, where the algorithm ran-
1149 domly chooses a candidate for the next sample value \mathbf{x}' based on
1150 the current sample value \mathbf{x}_t . The choice follows the proposal den-
1151 sity function, $\mathbf{x}' \sim Q(\mathbf{x}'|\mathbf{x}_t)$. When the proposal density Q is
1152 symmetric, for example a Gaussian, the sequence of samples is a
1153 random walk. In general the width of Q should match with the
1154 statistics of the distribution being sampled, and individual dimen-
1155 sions in the sampling space may behave differently in the multi-
1156 variate case; finding the appropriate Q can be difficult.

The proposed move is either accepted or rejected with some
1157 probability; if rejected, the current sample value is reused in the
1158 next iteration, $\mathbf{x}' = \mathbf{x}_t$. The probability of acceptance is deter-
1159 mined by comparing the values of $P(\mathbf{x}_t)$ and $P(\mathbf{x}')$, where $P(\mathbf{x})$ is
1160 the distribution being sampled. Because the algorithm only consid-
1161 ers the acceptance ratio $\rho = P(\mathbf{x}')/P(\mathbf{x}_t) = f(\mathbf{x}')/f(\mathbf{x}_t)$ where
1162 $f(\mathbf{x})$ can be any function proportional to the desired distribution
1163 $P(\mathbf{x})$, there is no need to worry about the proper normalization
1164 of the probability distribution. If $\rho \geq 1$, the move is always ac-
1165 cepted; if $\rho < 1$, it is accepted with a probability ρ . Consequently
1166 the samples tend to stay in the high-density regions, visiting the
1167 low-density regions only occasionally.

Optimizing the sampler. One of the major difficulties in using
1170 the MCMC method is to make an appropriate choice of the pro-
1171 posal distribution, which may significantly affect the performance
1172 of the sampler. If the proposal distribution is too narrow, it will
1173 take a long time for the chain to diffuse away from the starting
1174 point, producing a chain with highly correlated samples, requiring
1175 a long time to achieve independent samples. On the other hand if
1176 the proposal distribution is too wide, most of the proposed moves
1177 would be rejected, once again resulting in the chain stuck at the ini-
1178 tial point. In either case the chain would “mix” poorly (Rosenthal,
1179 2011). In this paper we restrict our consideration to the Metropolis-
1180 Hastings algorithm (Metropolis et al., 1953), although the issue of
1181 proposal distribution optimization is universal in most variants of
1182 MCMC algorithms, only with implementation-level differences.

The basic idea is that the optimal width of the proposal distribu-
1184

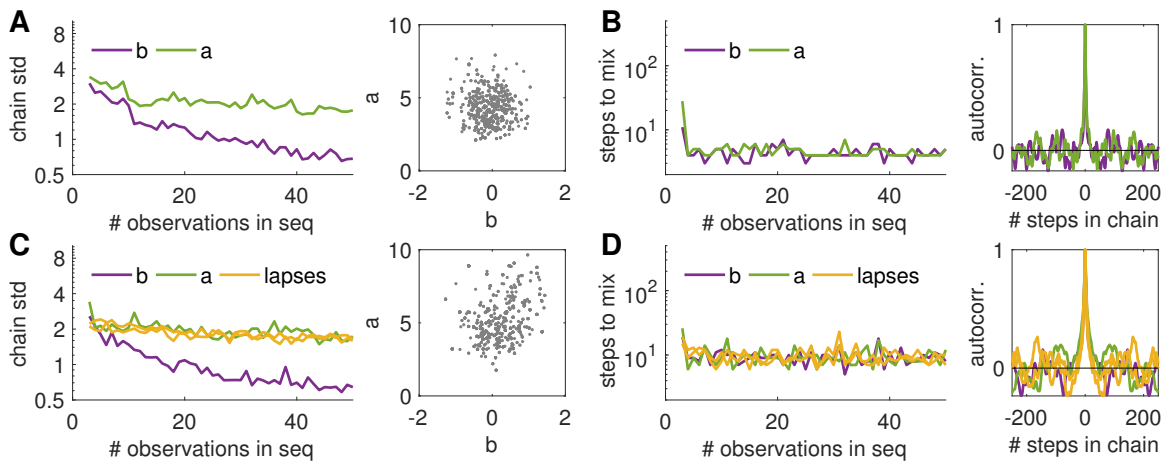


Figure 7: Statistics of the semi-adaptive MCMC in a simulated experiment, with $M = 1000$ samples per chain. We used the same binomial model as in Fig. 2, and the uniform stimulus selection algorithm. **(A-B)** In a lapse-free model: **(A)** The standard deviation of the samples, along each dimension of the parameter space, decreases as the learning progresses, as expected because the posterior distribution should narrow down as more observations are collected. Also shown is the scatter plot of all 1000 samples at the last trial $N = 50$, where the true parameter values are $(a, b) = (5, 0)$. **(B)** The mixing time of the chain (number of steps before the autocorrelation falls to $1/e$) quickly converges to some small value, meaning that the sampler is quickly optimized. Autocorrelation function at the last trial $N = 50$ is shown. **(C-D)** Same information as **(A)** and **(B)**, but with a lapse rate of $\lambda = 0.1$, with uniform lapse ($c_1 = c_2 = 1/2$).

1185 tion would be determined in proportion to the typical length scale
 1186 of the distribution being sampled. This idea was made precise in
 1187 the case of a stationary random-walk Metropolis algorithm with
 1188 Gaussian proposal distributions, by comparing the covariance ma-
 1189 trix Σ_p of the proposal distribution to the covariance matrix Σ of
 1190 the sampled chain. Once a linear scaling relation $\Sigma_p = s_d \Sigma$ is
 1191 fixed, it was observed that it is optimal to have $s_d = (2.38)^2/d$
 1192 where d is the dimensionality of the sampling space (Gelman et
 1193 al., 1996; Roberts et al., 1997). An adaptive Metropolis algo-
 1194 rithm (Haario et al., 2001) followed this observation, where the
 1195 Gaussian proposal distribution adapts continuously as the sampling
 1196 progresses. Their adaptive algorithm used the same scaling rule
 1197 $\Sigma_p = s_d \Sigma$, but updates Σ_p at each proposal where Σ is covariance
 1198 of the samples accumulated so far. Additionally, a small diagonal
 1199 component was added for stability, as $\Sigma_p = s_d(\Sigma + \epsilon I)$. We used
 1200 $\epsilon = 0.0001$ in this work.

1201 Here we propose and use the semi-adaptive Metropolis-Hastings
 1202 algorithm, which is a coarse-grained version of the original adap-
 1203 tive algorithm by Haario et al. (2001). The major difference in

our algorithm is that the adjustment of the proposal distribution is
 made only at the end of each (sequential) chain, rather than at each
 proposal within the chain. This coarse-graining is a reasonable ap-
 proximation because we will be sampling the posterior distribution
 many times as it refines over the course of data collection, once
 after each trial. Assuming that the change in posterior distribu-
 tion after each new observation is small enough, we can justify our
 use of the statistics of the previous chain to adjust the properties
 of the current chain. Unlike in the fully adaptive algorithm where
 the proposal distribution needs to stabilize quickly within a single
 chain, we can allow multiple chains until stabilization, usually a
 few initial observations – leaving some room for the coarse-grained
 approximation. This is because, for our purpose, it is not impera-
 tive that we have a good sampling of the distribution at the very
 early stage of the learning sequence where the accuracy is already
 limited by the smallness of the dataset.

When applied to the sequential learning algorithm, our semi-
 adaptive Metropolis sampler shows a consistent well-mixing prop-
 erty after a few initial adjustments, with the standard deviation

of each sampling dimension decreasing stably as data accumulate (Fig. 7). Whereas Kujala and Lukka (2006) also had the idea of adjusting the proposal density between trials, their scaling factor was fixed and independent of the sampling dimension. Building on more precise statistical observations, our method generalize well to high-dimensional parameter spaces, typical for multiple-alternative models. Our semi-adaptive sampler provides an efficient and robust alternative to the particle filter implementations (Kujala & Lukka, 2006), which has the known problem of weight degeneration (DiMattina, 2015) as the posterior distribution narrows down with the accumulation of data.

Appendix C

Fast sequential update of the posterior, with Laplace approximation.

Use of Laplace approximation was shown to be particularly useful in a sequential experiment (Lewi et al., 2009), where it can be assumed that the posterior distribution after the next trial in sequence, \mathcal{P}_{t+1} , would not be very different from the current posterior \mathcal{P}_t . Let us consider the lapse-free case $\theta = \mathbf{w}$ for the moment, where the use of Laplace approximation is valid. Rearranging from (7) and (9), the sequential update for the posterior distribution is

$$\log \mathcal{P}_{t+1}(\mathbf{w}) = \log \mathcal{P}_t(\mathbf{w}) + L_{t+1}(\mathbf{w}); \quad (47)$$

or with Laplace approximation,

$$\log \mathcal{N}(\mathbf{w}|\theta_{t+1}, C_{t+1}) \approx \log \mathcal{N}(\mathbf{w}|\theta_t, C_t) + L_{t+1}(\mathbf{w}) \quad (48)$$

where $L_i(\mathbf{w}) = \log p(\mathbf{y}_i|\mathbf{x}_i, \mathbf{w})$ is a shorthand for the log likelihood of the i -th observation.

With this, we can achieve a fast sequential update of the posterior without performing the full numerical optimization each time. Because the new posterior mode θ_{t+1} is where the gradient vanishes, it can be approximated from the previous mode θ_t by taking the first derivative of (48). The posterior covariance C_{t+1} is similarly

approximated by taking the second derivative.

$$\theta_{t+1} = \theta_t + C_t \Delta_{t+1}, \quad \Delta_{t+1} = \left. \frac{\partial L_{t+1}}{\partial \mathbf{w}} \right|_{\mathbf{w}=\theta_t} \quad (49)$$

$$C_{t+1} = (C_t^{-1} + \Lambda_{t+1})^{-1}, \quad \Lambda_{t+1} = - \left. \frac{\partial^2 L_{t+1}}{\partial \mathbf{w}^2} \right|_{\mathbf{w}=\theta_{t+1}} \quad (50)$$

Using the matrix inversion lemma (Henderson & Searle, 1981), we can rewrite the posterior covariance update as

$$C_{t+1} = C_t [I - (I + \Lambda_{t+1} C_t)^{-1} \Lambda_{t+1} C_t]. \quad (51)$$

Unlike in the earlier application of this trick (Lewi et al., 2009), the covariance matrix update (50) is not a rank-one update, because of the multinomial nature of our model (our linear predictor \mathbf{y} is a vector, not a scalar as in a binary model).

Note that this approximate sequential update is only used for calculating the expected utility of each candidate stimulus by approximating the posterior distribution at the next trial, as in Section Adaptive Stimulus Selection Methods. For obtaining the MAP estimates of the model parameters, numerical optimization should be performed using the full accumulated dataset each time.

Integration over the parameter space: reducing the integration space.

The evaluation of expected utility function usually involves a potentially high-dimensional integral over the parameter space. With the Gaussian approximation of the posterior, we can reduce and standardize the integration space. The process consists of three steps: diagonalization, marginalization, and standardization. First we choose a new “coordinate system” of the (say q -dimensional) weight space, such that the first k elements of the extended weight vector \mathbf{w} are coupled one-to-one to the elements of k -vector \mathbf{y} . Then we marginalize to integrate out the remaining $(q - k)$ dimensions, effectively changing the integration variable from \mathbf{w} to \mathbf{y} . Finally, we use Cholesky decomposition to standardize the normal distribution which is the posterior on \mathbf{y} . The resulting integral is still multi-dimensional, due to the multinomial nature of our model. But once the distribution is standardized, there are a number of efficient numerical integration methods that can be applied. For example, in this work, we use the Sparse Grid method (Heiss & Winschel, 2008) based on Gauss-Hermite quadrature.

1289 **Diagonalization.** It is clear from (19-20) and (29-30) that all
 1290 parameter-dependence in our integrand is in terms of the linear
 1291 predictor $\mathbf{y} = X\mathbf{w}$. That is, we are dealing with the integral of
 1292 the form

$$1293 \quad F = \int d\mathbf{w}' \mathcal{N}(\mathbf{w}'|\hat{\mathbf{w}}', C) \cdot f(X\mathbf{w}'), \quad (52)$$

1294 where C is the covariance matrix, and $X = \bigoplus_{j=1}^k \mathbf{g}'_j^\top$ is a fixed
 1295 matrix constructed from direct sum of k vectors. It helps to work
 1296 in a diagonalized coordinate system, so that we can separate out the
 1297 relevant dimensions of \mathbf{w} . We use the singular value decomposi-
 1298 tion of the design matrix ($X = UGV^\top$ with $U = I$ and $V = Q^\top$).
 1299 Because of the direct-sum construction, XX^\top is already diagonal,
 1300 and the left singular matrix is always I in this case. Then

$$1301 \quad G = XQ^\top = \begin{bmatrix} G_k & G_q \end{bmatrix}, \quad (53)$$

1302 where G_k is a $k \times k$ diagonal matrix and G_q is a $k \times (q - k)$
 1303 matrix of zeros. We can now denote $\mathbf{w}_k = (w_1, \dots, w_k)$ and
 1304 $\mathbf{w}_q = (w_{k+1}, \dots, w_q)$ in the diagonalized variable $\mathbf{w} = Q\mathbf{w}'$,
 1305 such that

$$1306 \quad \mathbf{w} = [\mathbf{w}_k, \mathbf{w}_q]^\top, \quad G\mathbf{w} = G_k\mathbf{w}_k = (g_1w_1, g_2w_2, \dots, g_kw_k).$$

1307 **Marginalization.** Now we have

$$1308 \quad F = \int d\mathbf{w} \mathcal{N}(\mathbf{w}|\hat{\mathbf{w}}, B^{-1}) \cdot f(G\mathbf{w}), \quad B^{-1} = QCC^\top \quad (54)$$

1309 where B is the inverse of the *new* covariance matrix after diagonal-
 1310 ization. If we block-decompose this matrix,

$$1311 \quad B = \begin{bmatrix} B_{kk} & B_{kq} \\ B_{qk} & B_{qq} \end{bmatrix}, \quad B_{kq} = (B_{qk})^\top, \quad (55)$$

1312 the Gaussian distribution is also decomposed as

$$1313 \quad \mathcal{N}(\mathbf{w}|\hat{\mathbf{w}}, B^{-1}) = \mathcal{N}(\mathbf{w}_k|\hat{\mathbf{w}}_k, B_*^{-1}) \cdot \mathcal{N}(\mathbf{w}_q|(\hat{\mathbf{w}}_q - \mathbf{b}), B_{qq}^{-1})$$

1314 where $\mathbf{b} = B_{qq}^{-1}B_{qk}\mathbf{w}_k$ and $B_* = B_{kk} - B_{kq}B_{qq}^{-1}B_{qk}$. As the
 1315 non-parallel part \mathbf{w}_q is integrated out, we have marginalized the
 1316 integral. It is useful to recall that if a variable $\mathbf{w} \sim \mathcal{N}(\hat{\mathbf{w}}, C)$ is
 1317 Gaussian distributed, its linear transform $\mathbf{y} = X\mathbf{w}$ is also Gaus-
 1318 sian distributed as $\mathbf{y} \sim \mathcal{N}(\hat{\mathbf{y}}, \Sigma)$, with $\hat{\mathbf{y}} = X\hat{\mathbf{w}}$ and $\Sigma = XCX^\top$.

Changing the integration variable to $\mathbf{y} = G_k\mathbf{w}_k$ is then straight-
 forward:

$$1319 \quad F = \int d\mathbf{w}_k \mathcal{N}(\mathbf{w}_k|\hat{\mathbf{w}}_k, B_*^{-1}) \cdot f(G_k\mathbf{w}_k) \quad 1321$$

$$1322 \quad = \int d\mathbf{y} \mathcal{N}(\mathbf{y}|\hat{\mathbf{y}}, \Sigma) \cdot f(\mathbf{y}), \quad \Sigma = G_kB_*^{-1}G_k^\top. \quad (56) \quad 1323$$

1324 **Standardization.** Finally, in order to deal with the numerical in-
 1325 tegration, it is convenient to have the normal distribution standard-
 1326 ized. We can use the Cholesky decomposition for the covariance
 1327 matrix,

$$1328 \quad LL^\top = \Sigma_{t+1}, \quad (57) \quad 1329$$

such that the new variable $\boldsymbol{\theta} = L^{-1}(\mathbf{y} - \hat{\mathbf{y}}_{t+1})$ is standard normal
 1330 distributed. From the above formulation, L can be written directly
 1331 in terms of the Cholesky decomposition of B_* :

$$1332 \quad L = G_kR^{-1} \quad \text{where} \quad R^\top R = B_*. \quad (58) \quad 1333$$

1334 Importantly, with this transformation, each dimension of $\boldsymbol{\theta}$ is inde-
 1335 pendently and identically distributed. The objective function to be
 1336 evaluated is now

$$1337 \quad F(\mathbf{x}) = \int d\mathbf{y} \cdot \mathcal{N}(\mathbf{y}|\hat{\mathbf{y}}_{t+1}, \Sigma_{t+1}) \cdot f(\mathbf{y}, \mathbf{x}) \quad 1338$$

$$1339 \quad = \int d\boldsymbol{\theta} \cdot \mathcal{N}(\boldsymbol{\theta}|\mathbf{0}, I) \cdot f(\phi(\boldsymbol{\theta}), \mathbf{x}) \quad (59) \quad 1340$$

1341 where $\phi(\boldsymbol{\theta}) = \hat{\mathbf{y}}_{t+1} + L\boldsymbol{\theta}$. Once the integration is standardized this
 way, there are a number of efficient numerical methods that can be
 applied.